

Contract No. DTFACT-15-D-00007
Task Order Number 005

DELIVERABLE 4.9.3.2
CC7 Post Traffic Report – Material Characterization.

August 20, 2019

Composed by:
Gemini Technologies Inc., for General Dynamics Information Technology

GENERAL DYNAMICS
Information Technology

TABLE OF CONTENTS

	Page
1. INTRODUCTION	1
2. OBJECTIVE	1
3. LABORATORY TESTING PROGRAM	1
3.1 P-401 HOT MIX ASPHALT AND ASPHALT TREATED DRAINABLE BASE (ATDB)	1
3.1.1 Asphalt Pavement Analyzer	1
3.1.2 Dynamic Modulus	1
3.1.3 Flow Number	2
3.1.4 High Temperature Indirect Tensile Strength (IDTH)	2
3.1.5 Tensile Strength Ratio	3
3.1.6 Falling Head Permeability Test	3
3.2 P-209 AGGREGATE BASE AND P-154 SUBBASE MATERIAL	4
3.3 P-152 SUBGRADE SOIL	5
4. P-401 HOT MIX ASPHALT AND ASPHALT TREATED DRAINABLE BASE (ATDB)	6
4.1 SAMPLE COLLECTION	6
4.2 TEST RESULTS	6
4.2.1 P-401 Characterization Tests	8
4.2.2 ATDB Characterization Tests	18
4.3 OBSERVATIONS	23
5. P-209 AGGREGATE BASE AND P-154 SUBBASE MATERIAL	23
5.1 SAMPLE COLLECTION	23
5.1.1 Triaxial Specimen Preparation	23
5.2 TEST RESULTS	26
5.2.1 Grain Size Distribution	26
5.2.2 Triaxial Test	39
5.3 OBSERVATIONS	53
6. P-152 SUBGRADE SOIL	54

6.1 SAMPLE COLLECTION	54
6.1.1 Triaxial Specimen Preparation	54
6.2 TEST RESULTS	54
6.3 OBSERVATIONS	57
7. REFERENCES	57
APPENDICES	

LIST OF FIGURES

Figure	Page
1 CC7 Layout and Cross-Sections	0
2 Schematic of Cumulative Permanent Strain vs. Loading Cycles – FN Test (7)	2
3 Permeability Test on ATDB	3
4 CC7 Post-Traffic Coring Locations	6
5 ATDB Test Slab (Non-Trafficked)	7
6 ATDB Test Slab (Trafficked)	7
7 APA Test Results for North side (-5 offset) at 100 psi and 147 °F	9
8 APA Test Results for North side (-25 offset) at 100 psi and 147 °F	9
9 APA Test Results for North side (-5 offset) at 250 psi and 147 °F	10
10 APA Test Results for North side (-25 offset) at 250 psi and 147 °F	10
11 APA Test Results for South side (-5 offset) at 100 psi and 147 °F	11
12 APA Test Results for South side (-5 offset) at 250 psi and 147 °F	11
13 Dynamic Modulus Master Curves	14
14 IDTH Load vs. Displacement Curves for North and South Sides	16
15 TSR Specimens	18
16 APA Test Results for ATDB at 100 psi and 147°F	19
17 APA Test Results for ATDB at 250 psi and 147°F	19
18 Comparison of Dynamic Modulus Master Curves for P-401 and ATDB	22
19 CC7 Trenching and Sampling Layout, 2017	24
20 CC7 Locations for Additional P-209 Sampling, 2018	25
21 Post-Traffic GSD of P-209 Base from LFC4-S, LFC5-S, and LFC6-S, South Side	27
22 Post-Traffic Average GSD of P-209 Base from LFC4-S, LFC5-S, and LFC6-S, South Side	28
23 G/S Ratio of P-209 Base from LFC4-S, LFC5-S, and LFC6-S, South Side	29
24 Post-Traffic GSD of P-154 Subbase from Perpetual Sections, North Side	31
25 Difference in GSD of P-154 Subbase Material among Perpetual Test Sections, North Side: (a) Percent Finer #200, (b) Percent Finer #40, (c) Percent Finer #10	32
26 Post-Traffic GSD of P-154 Subbase Material from Drainable Base Test Sections, North Side	33
27 Types of Aggregate Breakage (15)	34
28 Post-Traffic GSD of P-154 Subbase Material from LFC1-S, LFC2-S, and LFC3-S Test sections, South Side	35
29 Post-Traffic GSD of P-154 Subbase Material from LFC4-S, LFC5-S, and LFC6-S Test Sections, South Side	36
30 Comparison of Post-Traffic Fines content in P-154 Subbase Material for all Overload Test Sections, South Side	38
31 Comparison of Maximum Ruth Depth at Pass #14520 for all Overload Test Sections, South Side	38
32 Mohr-Coulomb Envelope for the South Side P-209 Material, LFC4-S Test Item	41
33 Relationship between G/S and Friction Angle for CC1 and CC7 Materials	42
34 Changes in Friction Angle for P-154 Material in Perpetual Sections, North Side	45
35 Effect of Overload Traffic on the Post-Traffic Maximum Vertical Stress: (a) LFC1-S to LFC3-S Test Sections, (b) LFC4-S to LFC6-S Test Sections	47
36 Comparison of Mohr-Coulomb Failure Envelopes for Post-Traffic P-154 Subbase: (a) LFC1-S to LFC3-S, (b) LFC4-S to LFC6-S	49

37 Changes in Friction Angle for P-154 Subbase in Overload Sections, South Side	50
38 Estimated Permanent Deformation from CC7 Post-Traffic Layer Profile Measurement	50
39 Changes in Friction Angle for P-154 Large Specimens (6×12 in.), South Side	52
40 Unconfined Compressive Strength of P-152 Subgrade: (a) North Side, (b) South Side	56

LIST OF TABLES

Table	Page
1 Laboratory Testing Program for HMA	1
2 Laboratory Testing Program for P-209 and P-154 Materials	4
3 Total Number of Triaxial Specimens Tested per Material	4
4 Laboratory Testing Program for P-152 Subgrade Soil	5
5 P-401 Gradation and Volumetrics	8
6 Summary of APA Test Results for North and South sides	12
7 Summary of Dynamic Modulus Test Results for P-401 Mixture (North Side)	15
8 Summary of TSR Test Results	17
9 Summary of APA Test Results for ATDB	18
10 Summary of Dynamic Modulus Test Results for Drainable Base	21
11 Results of Falling Head Permeability Test on ATDB	22
12 CC7 Post-Traffic GSD of P-209 Base, South Side	26
13 CC7 Post-Traffic GSD of P-154 Subbase from Perpetual Sections, North Side	30
14 CC7 Post-Traffic GSD of P-154 Material Drainable Base, North Side	33
15 CC7 Post-Traffic GSD of P-154 Subbase, South Side	37
16 Summary of Triaxial Test Results for P-209 Specimens	40
17 Summary of Strength Parameters for P-209 Specimens	42
18 Summary of Triaxial Test Results for P-154 Specimens, North Side	44
19 Summary of Strength Parameters for P-154 Specimens, North Side	44
20 Summary of Triaxial Test Results for P-154 Specimens, South Side	46
21 Summary of Strength Parameters for P-154 Specimens, South Side	48
22 Summary of Triaxial Test Results for Large P-154 Specimens (6×12 in.), South Side	51
23 Summary of Strength Parameters for Large P-154 Specimens (6×12 in.), South Side	52
24 Summary of Triaxial Test Results for P-152 Specimens, North and South Side	55

LIST OF ACRONYMS

2D	Dual Tandem
AC	Advisory Circular
ACN-PCN	Aircraft Classification Number–Pavement Classification Number
APA	Asphalt Pavement Analyzer ATDB
ATDB	Asphalt Treated Drainable Base
AV	Air Voids
CC1	Construction Cycle 1
CC7	Construction Cycle 7
CDF	Cumulative Damage Factor
D	Dual
FAA	Federal Aviation Administration
FN	Flow Number
GSD	Grain Size Distribution
G/S	Gravel-to-Sand Ratio
HMA	Hot-Mix Asphalt
ICAO	International Civil Aviation Organization
JMF	Job Mix Formula
LVDT	Linear Vertical Displacement Transducers
NAPTF	National Airport Pavement Test Facility
NAPTV	National Airport Pavement Test Vehicle
NCHRP	National Cooperative Highway Research Program
SCI	Structural Condition Index
TSR	Tensile Strength Ratio
UCS	Unconfined Compressive Strength
VMA	Voids in Mineral Aggregates

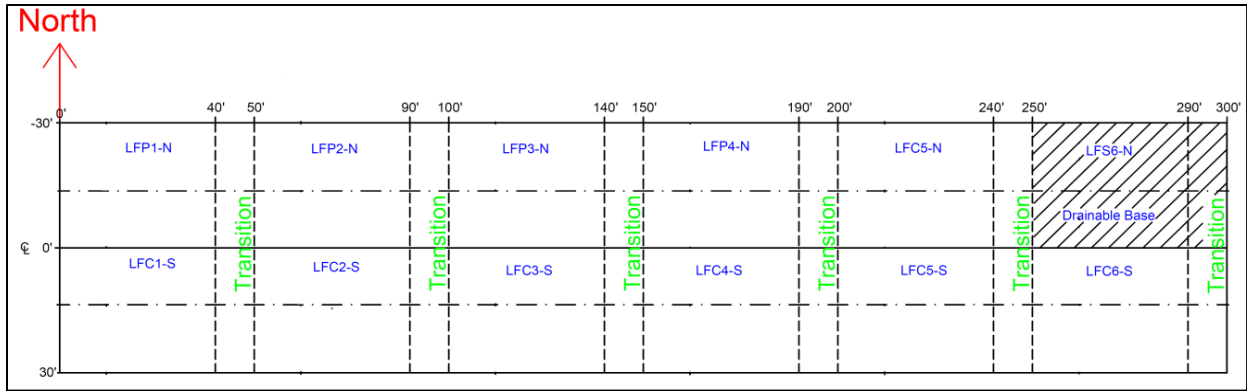
1. INTRODUCTION

Construction Cycle 7 (CC7) has been the most complex and challenging full-scale experiment ever conducted at the Federal Aviation Administration (FAA) National Airport Pavement Test Facility (NAPTF). A total of twelve fully instrumented pavement sections were built as part of the CC7 test track: six on the north and six on the south side (figure 1). On the north side, four test sections were designed for perpetual pavement tests, and two were designed to provide a control test section and evaluate the structural performance of Asphalt Treated Drainable Base (ATDB). On the south side, six test sections of constant cross-sections were built, aimed at studying overload effects and developing allowable overload criteria for airport asphalt pavements. A single Job Mix Formula (JMF) with two different binders was used in the construction of the hot mix asphalt (HMA [FAA specification P-401]) layer of CC7. For the south side test sections, a Performance Grade (PG) 64-22 binder was used, whereas, for the north side test sections, a PG 76-22 binder was used. The CC7 full-scale traffic test began on September 15, 2014 and concluded on December 8, 2016. The details on construction and full-scale traffic test of the CC7 pavement sections can be found in further literature (1-3).

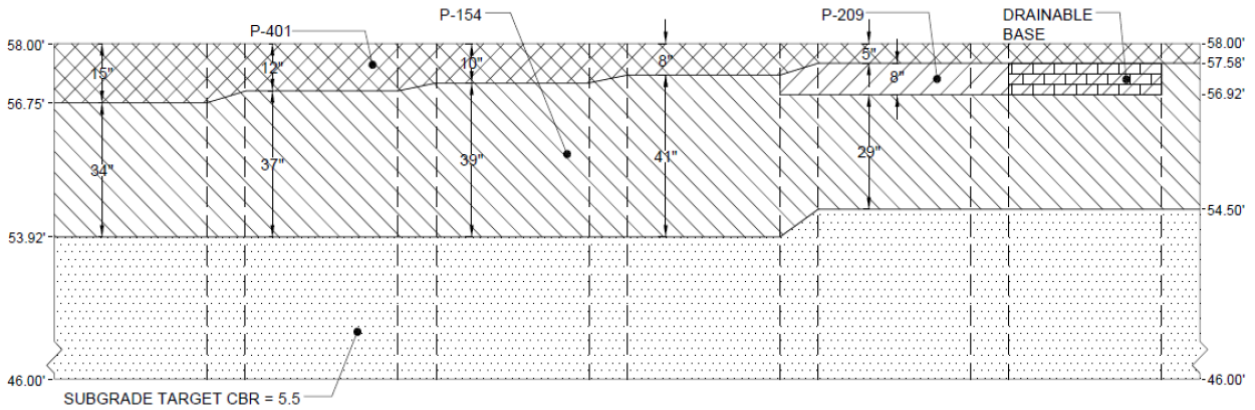
Post-traffic testing on CC7 pavement sections began in June 2017 and was completed in September of the same year. Trenches were excavated in all test sections and unbound material samples were collected from all the structural layers in order to conduct post-traffic testing at the FAA's NextGen Pavement Materials Laboratory. However, the P-209 aggregate base layer materials initially sampled was found to not represent the actual CC7 P-209 material gradation. Therefore, additional sampling of P-209 material was conducted later in August 2018. This report presents post-traffic laboratory testing and analysis of CC7 P-401 and unbound materials.

2. OBJECTIVE

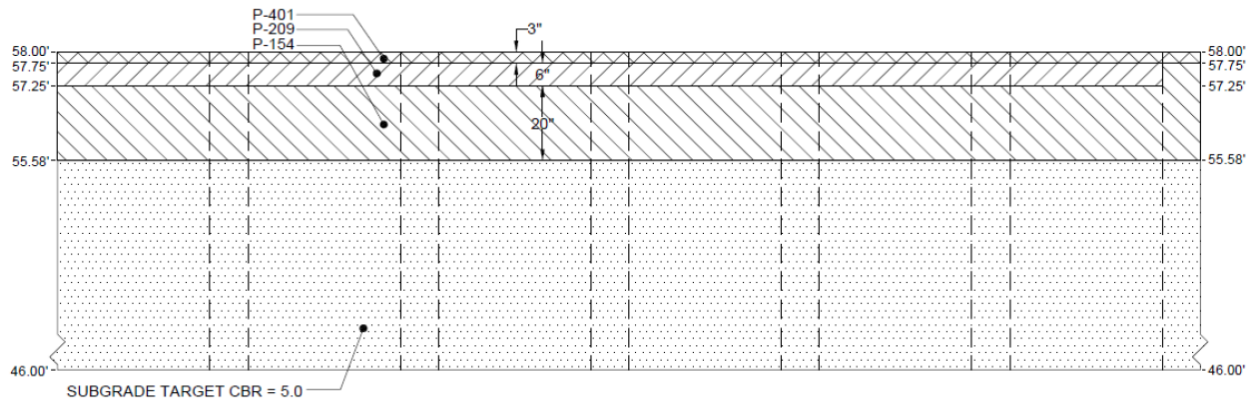
The objective of CC7 post-traffic characterization of P-401, P-209, P-154, and subgrade was in search for evidence of potential changes in material properties due to full-scale trafficking. For P-401 material, this was pursued by comparing laboratory test results from post-traffic samples with those from construction. For unbound materials, the effect of full-scale tests was investigated by comparing laboratory test results of samples collected from trafficked and non-trafficked areas.



(a) CC7 Layout



(b) Structural Layout of Perpetual Pavement Test Sections, North



(c) Structural Layout of Overload Pavement Test Sections, South

Figure 1. CC7 Layout and Cross-Sections

3. LABORATORY TESTING PROGRAM

3.1 P-401 HOT MIX ASPHALT AND ASPHALT TREATED DRAINABLE BASE (ATDB)

The laboratory testing program for P-401 material included asphalt pavement analyzer (APA), dynamic modulus, flow number, and high temperature indirect tensile strength (IDTH), Tensile Strength Ratio (TSR), and permeability test as shown in table 1.

Table 1. Laboratory Testing Program for HMA

Item	Property	Test	Standards	Quantities
P-401	Modulus	Dynamic Modulus	AASHTO TP79	3
	Permanent deformation	Flow Number	AASHTO TP79	3
		APA (100psi and 250psi)	AASHTO T340	12
	Moisture sensitivity	Tensile Strength Ratio	ASTM D4867	3
	Air Voids	Gmb and Gmm	ASTM D3203	3
ATDB	Modulus	Dynamic Modulus	AASHTO TP79	3
	Permanent deformation	APA (100psi and 254psi)	AASHTO T340	12
	Permeability	Falling Head Permeability Test	P-203	3
	Air Voids	Gmb and Gmm	ASTM D3203	3

3.1.1 Asphalt Pavement Analyzer

In flexible airport pavements, rutting has been a major distress under higher wheel loads and higher tire pressures (4). The APA features an automated data acquisition system, which obtains rutting measurements and displays these measurements in a numeric and/or graphical format (5). The test mimics the action of a heavily loaded, high tire pressure wheel moving on the HMA surface and has been used a pass/fail criterion for HMA field rutting performance by some transportation agencies (5). The recommended criteria for satisfactory rutting performance of HMA mixtures under aircraft high tire pressure is less than 0.39-inch (10-mm) APA rut depth after 4,000 cycles when tested with 250 psi hose pressure (6).

Six 3-inch height by 6-inch diameter APA samples were tested at 100 and 250 psi for both north and south side P-401 specimens. The APA tests were conducted at 147 °F with the cyclic load applied at the rate of one cycle per second. The terminal rut depth of the specimens was set at 0.47 inch (12 mm) or 10,000 cycles, whichever comes first.

3.1.2 Dynamic Modulus

Dynamic modulus test was conducted as per AASHTO TP79 *Determining the Dynamic Modulus and Flow Number for Asphalt Mixtures Using the Asphalt Mixture Performance Tester* for only the north side cores. Tests were performed at five temperatures: 14, 39, 70, 99, and 129°F using loading frequencies of 25, 10, 5, 1, 0.5, and 0.1 Hz. Dynamic modulus tests were conducted on three replicate specimens with a diameter of 4 inches and trimmed to the height of 6 inches.

3.1.3 Flow Number

The Flow Number (FN) test is a simple performance test related to permanent deformation of HMA mixtures. In the FN test, a repeated dynamic load is applied on the specimen in a sinusoidal wave for 0.1 sec, followed by a rest period of 0.9 sec. During the test axial strain is measured, the sample is loaded until tertiary flow.

A schematic of the test is provided in figure 2. As illustrated in figure 2, flow number corresponds to the minimum value of the rate of change of axial strain when plotted against the number of cycles on a log-log scale. FN tests were conducted at 126°F with deviator stress and contact stress of 200 psi and 5 psi respectively. The tests were conducted on the dynamic modulus specimens for the north side test sections and were continued until termination or 10,000 cycles, whichever came first. The termination was defined as reaching a microstrain level of 50,000.

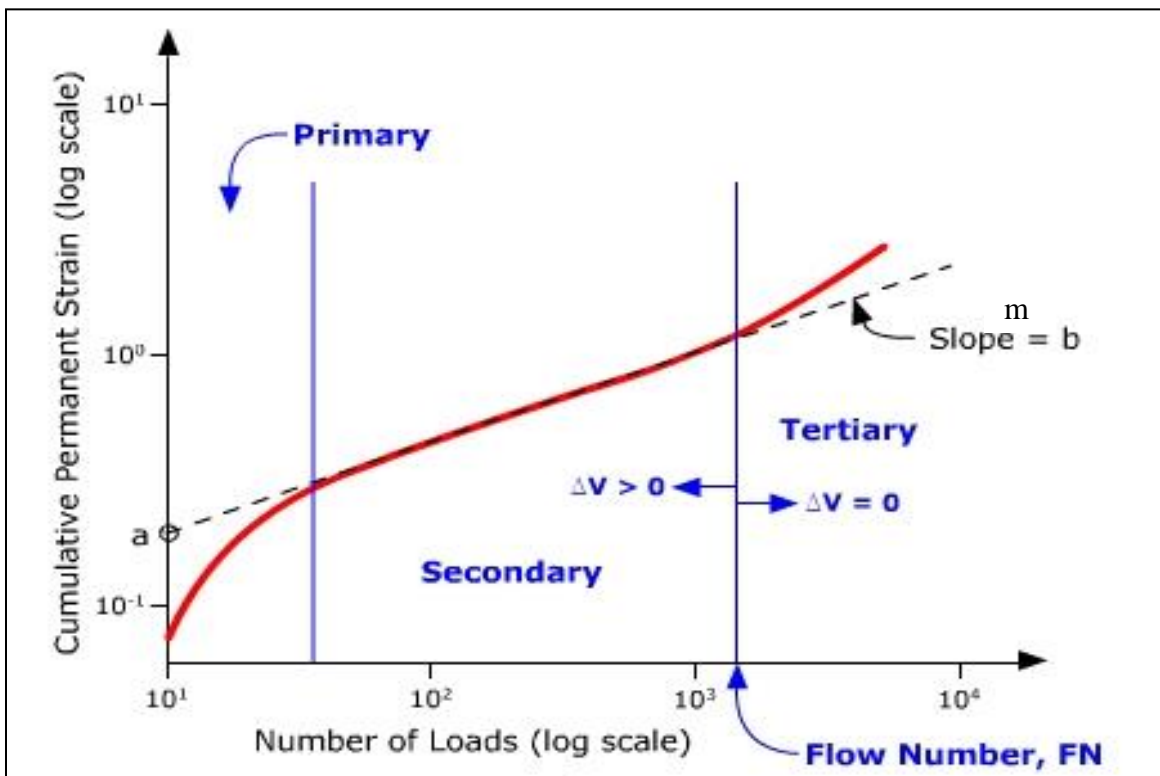


Figure 2. Schematic of Cumulative Permanent Strain vs. Loading Cycles – FN Test (7)

3.1.4 High Temperature Indirect Tensile Strength (IDTH)

High Temperature Indirect Tensile Strength (IDTH) test was conducted at 108°F for both north and south side cores. The specimens were 2.95 inches in height and 6 inches in diameter. Three replicates were tested for each side.

3.1.5 Tensile Strength Ratio

Tensile Strength Ratio (TSR) test was conducted as per ASTM D4867 “*Standard Test Method for Effect of Moisture on Asphalt Concrete Paving Mixtures*”. Field cores from both north and south sides were tested. At least six specimens (4 inches in diameter and 2.5 inches in height) were tested for each side, three in dry condition, and three in partial saturation/freezing and moisture conditioning.

3.1.6 Falling Head Permeability Test

FAA P-203 permeability testing procedure was followed. A 15-inch diameter rigid plastic cylinder, approximately 3 feet tall was placed on the test surface area, as shown in figure 40. Next, the test surface area was pre-wetted with 5 gallons of water for 20 seconds prior to conducting the test. Then, 5 gallons of water were then poured into the cylinder, directing the flow to the center. As soon as all water was drained from the cylinder, a second 5 gallons of water was poured. The elapsed time between the initial contact of this water with the drainage layer surface and the disappearance of water from the surface was measured. These steps were repeated four times with a 2-minute gap between each. The coefficient of permeability was computed using Equation 13.

$$k = 798.0725/C \quad \text{Equation 1}$$

where k is the coefficient of permeability (feet/day) and C is the time (minutes)



Figure 3. Permeability Test on ATDB

3.2 P-209 AGGREGATE BASE AND P-154 SUBBASE MATERIAL

Two tests were conducted on the P-209 and P-154 materials: 1) Grain Size Distribution (GSD) and 2) Resilient Modulus followed by a Quick Shear test. Determination of the GSD was achieved by performing ASTM C117 *Standard Test Method for Materials Finer than 75- μ m (No. 200) Sieve in Mineral Aggregates by Washing*, and ASTM C136 *Standard Test Method for Sieve or Screen Analysis of Fine and Coarse Aggregates*. The measurement of stiffness-strength was conducted in accordance with AASHTO T307 *Determining the Resilient Modulus of Soils and Aggregate Materials*. The resilient modulus test was performed on all specimens followed by the quick shear test at different levels of confining pressure. Table 2 summarizes the number of tests per test procedure. The information corresponding to advanced soil testing detailed in table 2 was condensed and presented in table 3. Also, note in table 3 that P-154 granular subbase specimens of two different triaxial specimen sizes were tested to investigate possible effects of specimen size and compaction method as explained later in section 5.2.2.4.

Table 2. Laboratory Testing Program for P-209 and P-154 Materials

Material	Section	Number of Tests					
		Particle Size Distribution (ASTM C117 & C136)		Resilient Modulus (AASHTO T307)		Quick Shear (AASHTO T307)	
		Trafficked	Non-Trafficked	Trafficked	Non-Trafficked	Trafficked	Non-Trafficked
P-154	LFP1-N	1	0	3	0	3	0
	LFP2-N	1	0	3	0	3	0
	LFP3-N	1	1	2	0	2	0
	LFP4-N	1	1	2	0	2	0
	LFC5-N	1	1	1	0	1	0
	LFS6-N	1	1	1	0	1	0
	LFC1-S	1	1	3	3	3	3
	LFC2-S	1	0	3	0	3	0
	LFC3-S	1	0	3	0	3	0
	LFC4-S	1	0	5	0	5	0
	LFC5-S	1	1	3	0	3	0
	LFC6-S	1	0	5	0	5	0
P-209	LFC4-S	3	3	3	3	3	3
	LFC5-S	3	0	3	0	3	0
	LFC6-S	3	3	3	3	3	3

Note: in the table, the numbers of tests conducted per procedure are indicated for each test section.

Table 3. Total Number of Triaxial Specimens Tested per Material

Material	Number of Specimens
P-209 (6 in. \times 12 in.)	15
P-154 (4 in. \times 8 in.)	33
P-154 (6 in. \times 12 in.)	4
Total	52

Two triaxial systems were used for advanced unbound material testing per AASHTO T307. The P-209 aggregate base specimens (6-inch diameter by 12-inch height) were tested using a large size electro-hydraulic triaxial system manufactured by MTS Systems Corporation. A medium size electro-pneumatic triaxial system manufactured by IPC Global was used to test P-154 granular subbase specimens (4-inch diameter by 8-inch height). Besides P-209 material, a limited number of P-154 specimens (6-inch diameter by 12-inch height) were tested with the MTS Systems Corporation equipment. The vertical deformations were measured by internal Linear Vertical Displacement Transducers (LVDT) in the MTS equipment whereas external LVDTs were used in the IPC system. In both systems, air was used as confining media.

3.3 P-152 SUBGRADE SOIL

For P-152 subgrade soil, only the Resilient Modulus followed by unconfined Quick Shear test was conducted. The measurement of stiffness-strength in subgrade soil was performed in accordance with AASHTO T307 *Determining the Resilient Modulus of Soils and Aggregate Materials*. As shown in table 4, total of 14 undisturbed P-152 subgrade Shelby tube specimens of 2.8-inch diameter by 5.6-inch height were tested using a medium size electro-pneumatic triaxial system manufactured by IPC Global. For the Resilient Modulus test, the vertical deformations were measured external LVDTs and air was used as confining media.

Table 4. Laboratory Testing Program for P-152 Subgrade Soil

		Number of Tests			
		Resilient Modulus (AASHTO T307)		Quick Shear (AASHTO T307)	
Material	Section	Trafficked	Non-Trafficked	Trafficked	Non-Trafficked
P-152	LFP1-N	1	0	1	0
	LFP2-N	1	0	1	0
	LFP3-N	1	1	1	1
	LFP4-N	1	0	1	0
	LFC5-N	1	0	1	0
	LFS6-N	1	0	1	0
	LFC1-S	1	0	1	0
	LFC2-S	1	0	1	0
	LFC3-S	1	0	1	0
	LFC4-S	1	0	1	0
	LFC5-S	1	0	1	0
	LFC6-S	1	1	1	1

Note: in the table, the numbers of tests conducted are indicated for each test section.

4. P-401 HOT MIX ASPHALT AND ASPHALT TREATED DRAINABLE BASE (ATDB)

4.1 SAMPLE COLLECTION

Post-traffic P-401 HMA material characterization tests were conducted on 6-inch cores extracted from the non-traffic area away from upheaval. The cores were collected from both north and south sides. The locations of these cores are shown in figure 4.

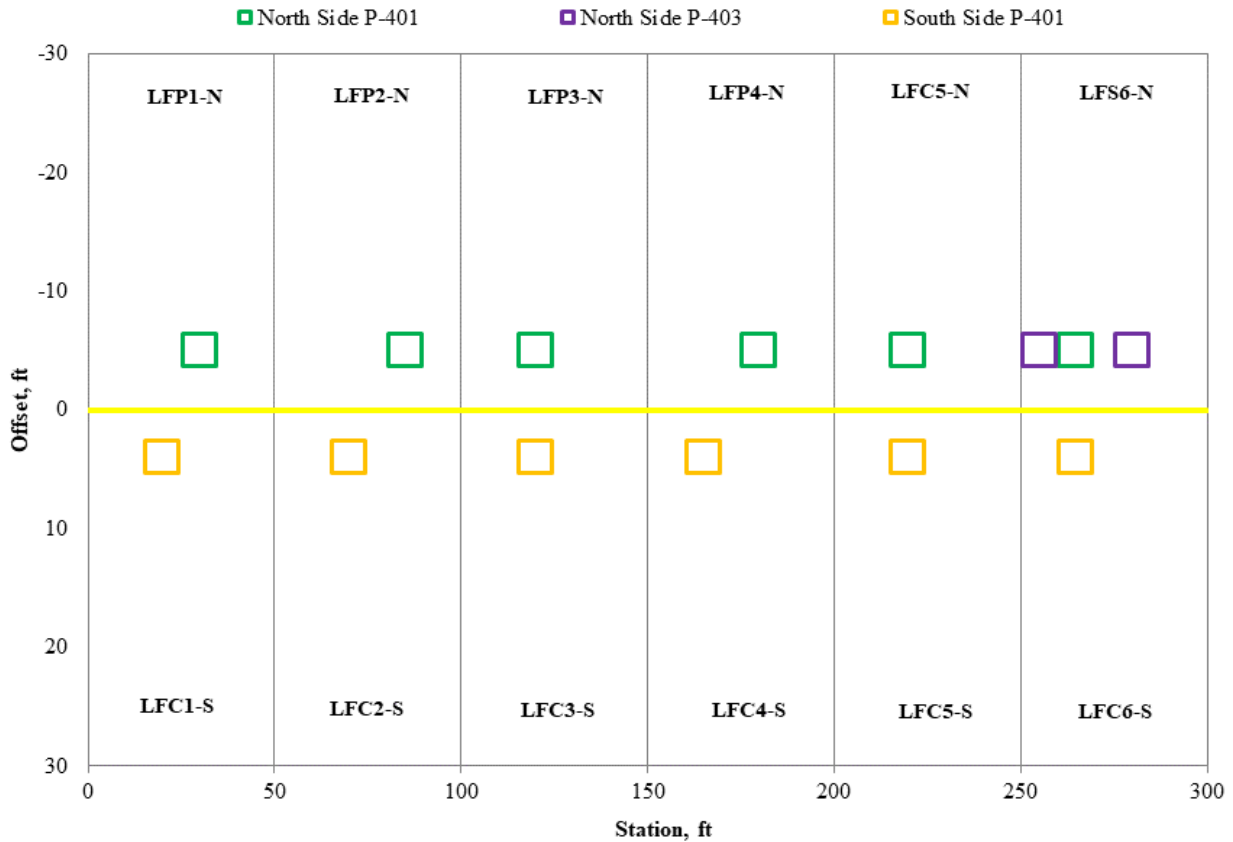


Figure 4. CC7 Post-Traffic Coring Locations

The post-traffic falling head permeability test was conducted on extracted 3x3-foot slabs of ATDB from the test section LFS-6N at station 2+75. In October 2018, these slabs were extracted from both non-trafficked (7.5-inch thick) and trafficked (6.6-inch thick) test areas, as shown in figures 5 and 6, respectively.

4.2 TEST RESULTS

The gradation and volumetrics of the two P-401 mixtures, following FAA Advisory Circular 150/5370-10C (8), are shown in table 5. Note that the pre-traffic specimens were prepared in the laboratory with a design target air void (AV) of ~3.5% using Superpave Gyratory Compactor (SGC). However, post-traffic cores from the non-traffic areas had higher AV (6-10% range).



Figure 5. ATDB Test Slab (Non-Trafficked)



Figure 6. ATDB Test Slab (Trafficked)

Table 5. P-401 Gradation and Volumetrics

Sieve Size	P-401		ATDB	
	Cumulative Percent Passing			
	Blended Aggregates	P-401 Spec	Blended Aggregates	ATDB Spec
3/4"	100.0	100.0	100	95-100
1/2"	95.4	79-99	91.0	85-100
3/8"	87.5	66-88	78.0	60-90
#4	62.9	48-68	20.0	15-25
#8	36.9	33-53	9.0	2-10
#16	22.3	20-40	6.05	-
#30	15.1	14-30	5.0	-
#50	11.8	9-21	4.0	-
#100	8.8	6-16	3.3	-
#200	5.8	3-6	2.7	2-5
Maximum Specific Gravity	2.621	-	2.622	-
Bulk Specific Gravity	2.530	-	2.066	-
Optimum Asphalt Content (%)	5.0	4.5-7.0	3.0	2.5-3.5
Air Voids (%)	3.5	2.8-4.2	21.2	-
VMA (%)	15.7	≥15.0	N/A	-

4.2.1 P-401 Characterization Tests

4.2.1.1 Asphalt Pavement Analyzer

APA test result are provided in figures 7 to 12 and table 6. For the north side, the APA samples were extracted from two different locations (-5 ft. offset [OS] and -25 ft. OS of centerline). As expected, the rut depth for the 250-psi test was higher than the 100 psi test. With the recommended criteria for satisfactory APA rutting performance being less than 10-mm rut depth after 4,000 cycles, both north and south side performed satisfactorily. The pre-traffic average APA rut depth after 4,000-wheel passes was 4-mm for both the north and south side (3).

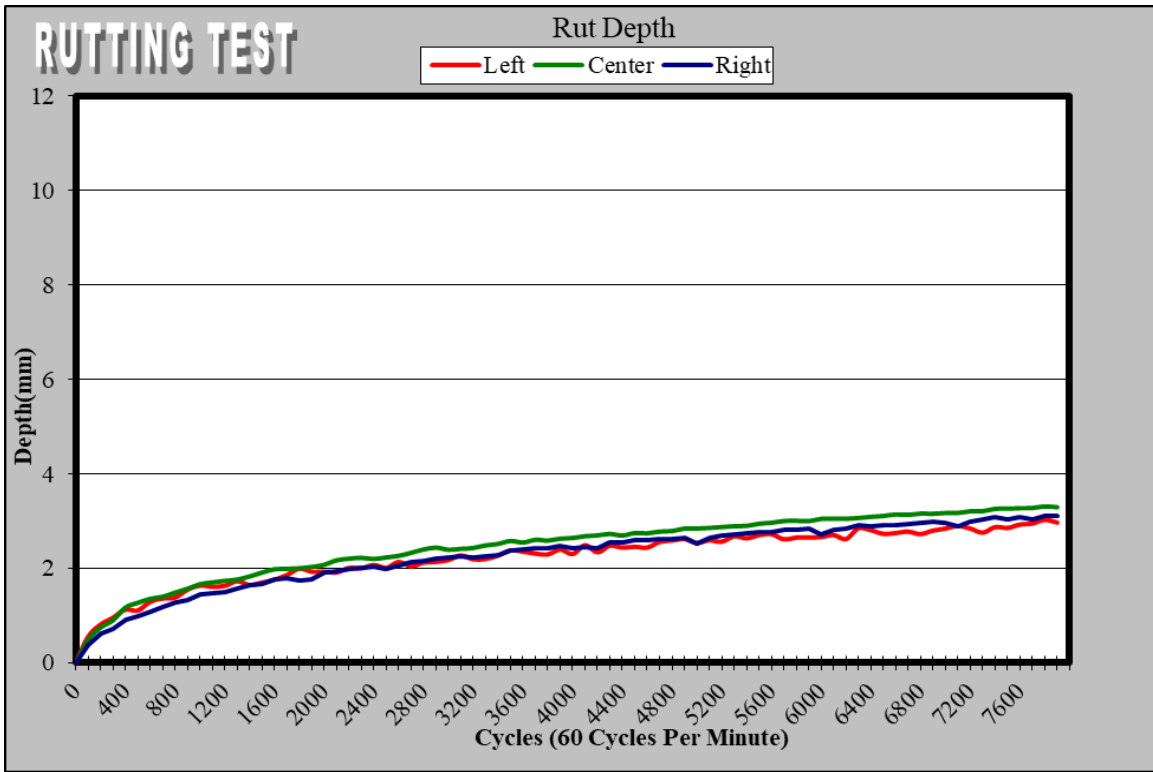


Figure 7. APA Test Results for North side (-5 offset) at 100 psi and 147 °F

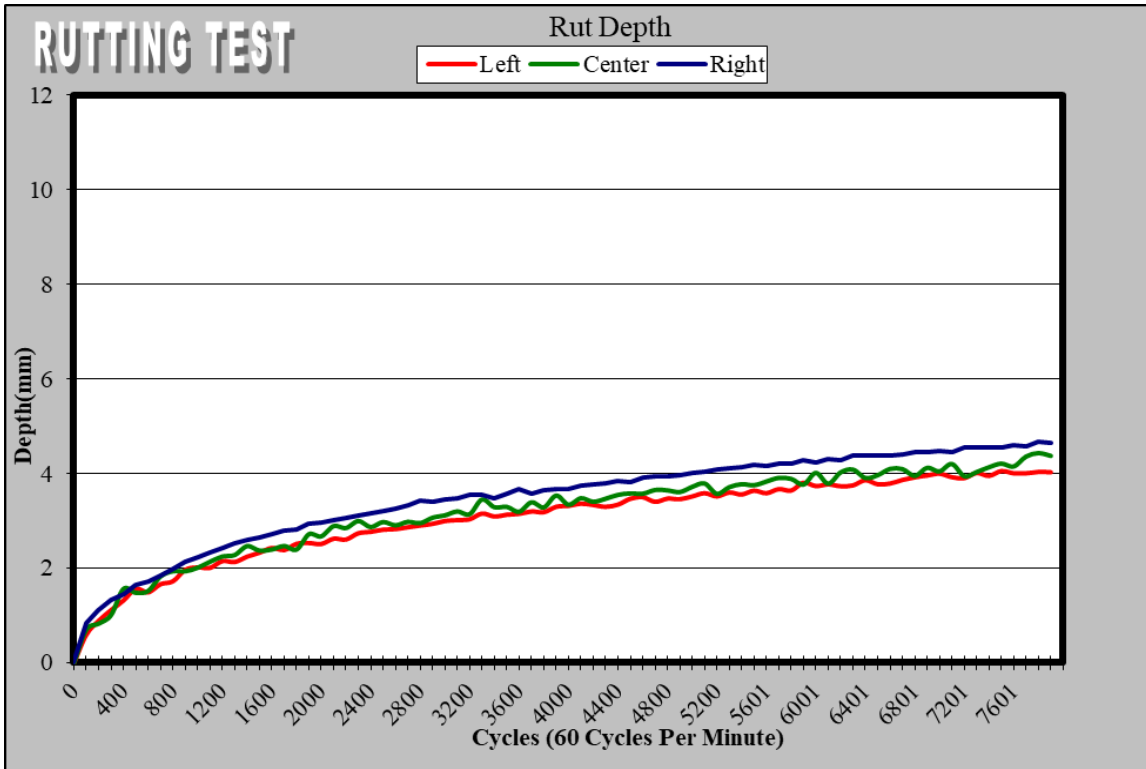


Figure 8. APA Test Results for North side (-25 offset) at 100 psi and 147 °F

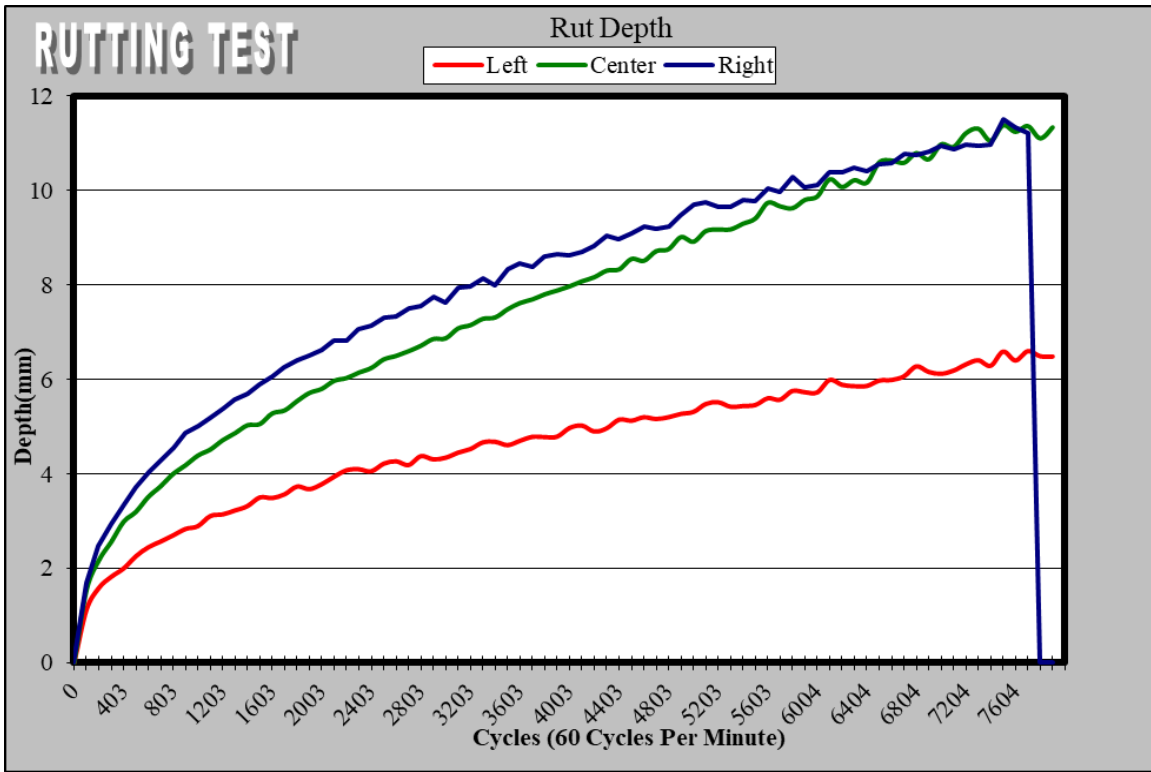


Figure 9. APA Test Results for North side (-5 offset) at 250 psi and 147 °F

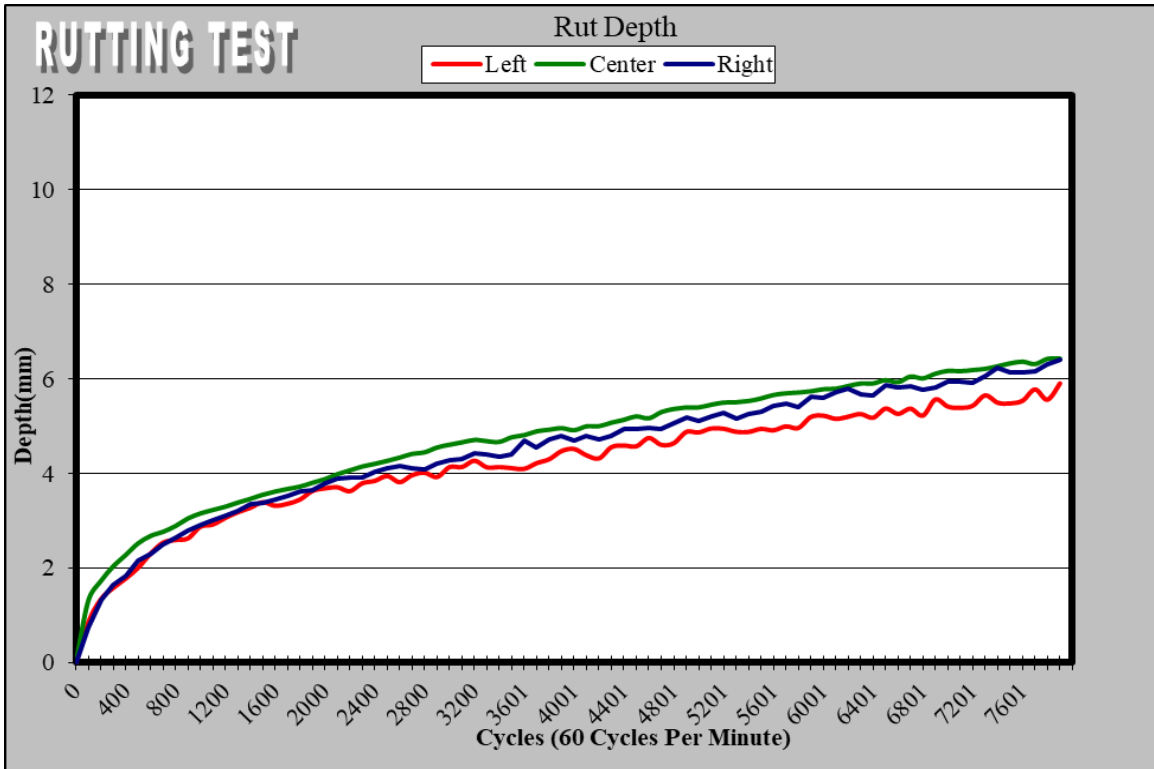


Figure 10. APA Test Results for North side (-25 offset) at 250 psi and 147 °F

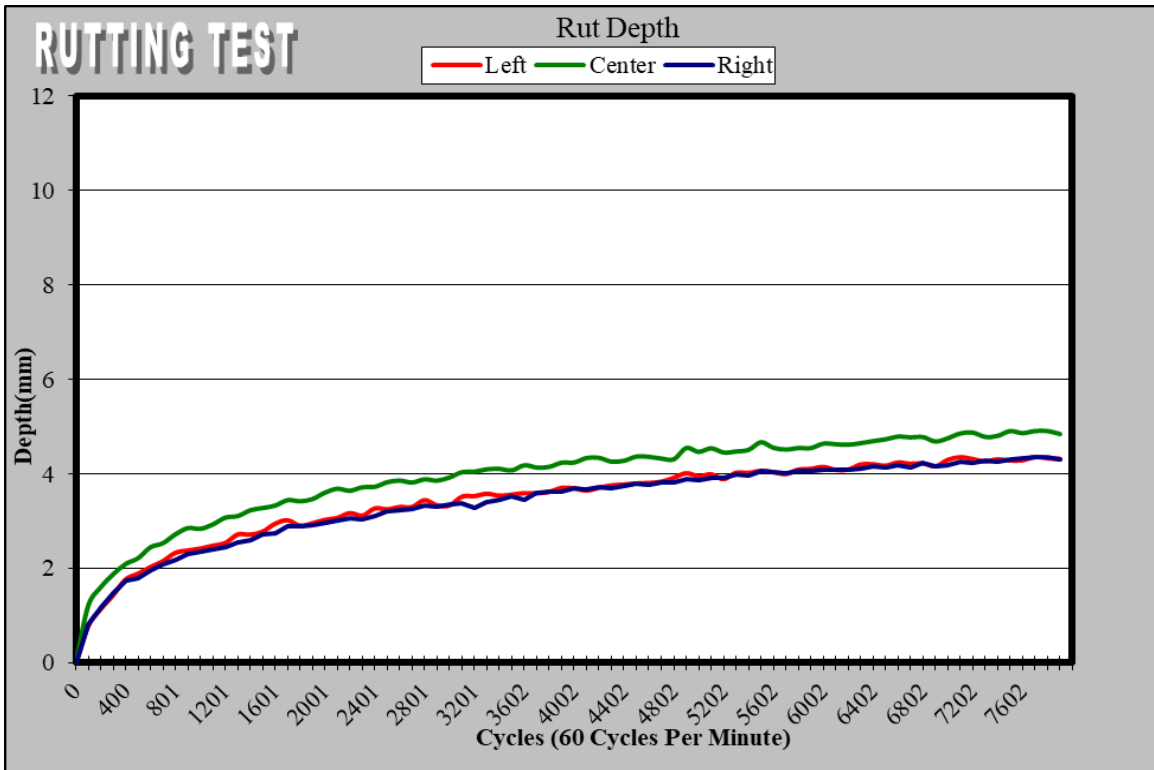


Figure 11. APA Test Results for South side (-5 offset) at 100 psi and 147 °F

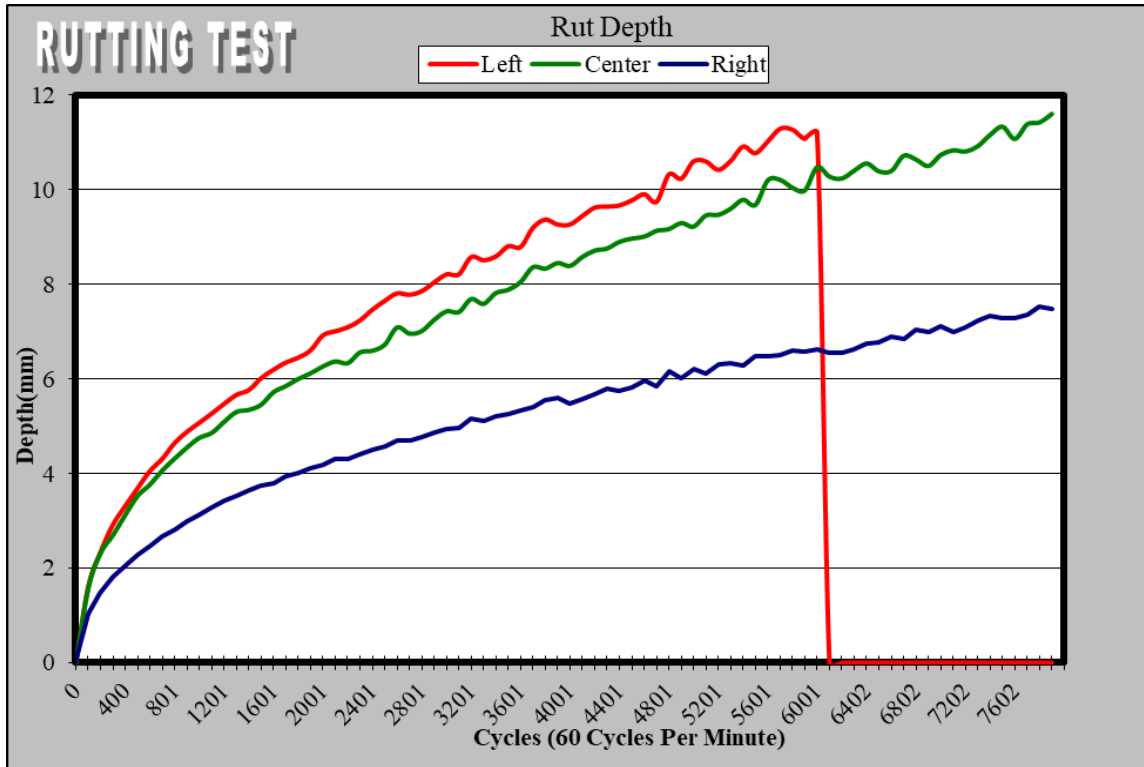


Figure 12. APA Test Results for South side (-5 offset) at 250 psi and 147 °F

Table 6. Summary of APA Test Results for North and South sides

Rut Depth (mm) @ 4000 cycles				
Wheel Location	Air Voids (%)	Left	Center	Right
North Side (PG 76-22)				
100 psi (-5 OS)	8.4	2.31	2.65	2.43
250 psi (-5 OS)	9.5	4.88	8.06	8.89
100 psi (-25 OS)	6.7	3.32	3.34	3.68
250 psi (-25 OS)	5.4	4.57	4.96	4.65
South Side (PG 64-22)				
100 psi	5.0	3.63	4.22	3.62
250 psi	5.9	9.43	8.50	5.58

4.2.1.2 Dynamic Modulus

For graphical analysis and easy interpretation of test data, $|E^*|$ master curves were generated by shifting data according to the time-temperature superposition principle described in Equation 2 (9):

$$\log|E^*| = \log(\text{Min}) + \frac{(\log(\text{Max}) - \log(\text{Min}))}{1 + e^{\beta + \gamma \log \omega_r}} \quad \text{Equation 2}$$

where $|E^*|$ is dynamic modulus (ksi), ω_r is reduced frequency (Hz), Max is limiting maximum modulus (ksi), Min is limiting minimum modulus (ksi), and β and γ are fitting parameters. The reduce frequency is computed using the Arrhenius equation, provided in equation 3:

$$\log \omega_r = \log \omega + \frac{\Delta E_a}{19.14714} \left(\frac{1}{T} - \frac{1}{T_r} \right) \quad \text{Equation 3}$$

where ω_r is reduced frequency at the reference temperature (Hz), ω is loading frequency at the test temperature (Hz), T_r is reference temperature (°F). T is test temperature (°F), and ΔE_a is activation energy (treated as a fitting parameter). Substituting Equation 3 into Equation 2 yields the form of the master curve equation, as provided in Equation 4:

$$\log|E^*| = \log(\text{min}) + \frac{(\log(\text{Max}) - \log(\text{Min}))}{1 + e^{\beta + \gamma \left\{ \log \omega + \frac{\Delta E_a}{19.14714} \left[\left(\frac{1}{T} \right) - \left(\frac{1}{T_r} \right) \right] \right\}}} \quad \text{Equation 4}$$

Shift factors for each temperature are provided in Equation 5:

$$\log[a(T)] = \frac{\Delta E_a}{19.14714} \left(\frac{1}{T} - \frac{1}{T_r} \right) \quad \text{Equation 5}$$

where $\alpha(T)$ is shift factor at temperature T . The maximum limiting modulus is estimated from mixture volumetric properties using the Hirsch model and a limiting binder modulus of 145,000 psi, as provided in Equations 6 and 7:

$$|E^*|_{\max} = P_c \left[4,200,000 \left(1 - \frac{VMA}{100} \right) + 435,000 \left(\frac{VFA \times VMA}{10,000} \right) \right] + \frac{1 - P_c}{\left[\frac{\left(1 - \frac{VMA}{100} \right)}{4,200,000} + \frac{VMA}{435,000(VFA)} \right]} \quad \text{Equation 6}$$

$$P_c = \frac{\left(20 + \frac{435,000(VFA)}{VMA} \right)^{0.58}}{650 + \left(\frac{435,000(VFA)}{VMA} \right)^{0.58}} \quad \text{Equation 7}$$

where $|E^*|_{\max}$ is limiting maximum mixture dynamic modulus, VMA is voids in mineral aggregates (%), and VFA is voids filled with asphalt (%). In developing dynamic modulus master curves, VMA for this mixture was 15.7% (table 16) and VFA was calculated using Equation 8:

$$VFA = \frac{VMA - V_a}{VMA} \quad \text{Equation 8}$$

where V_a is air void content of the compacted sample. Figure 13 provides the master curves developed at a reference temperature of 70°F. For comparison purpose, the pre-traffic master curve is also plotted in the same figure. The modulus and phase angle at different temperatures and frequencies are presented in table 7.

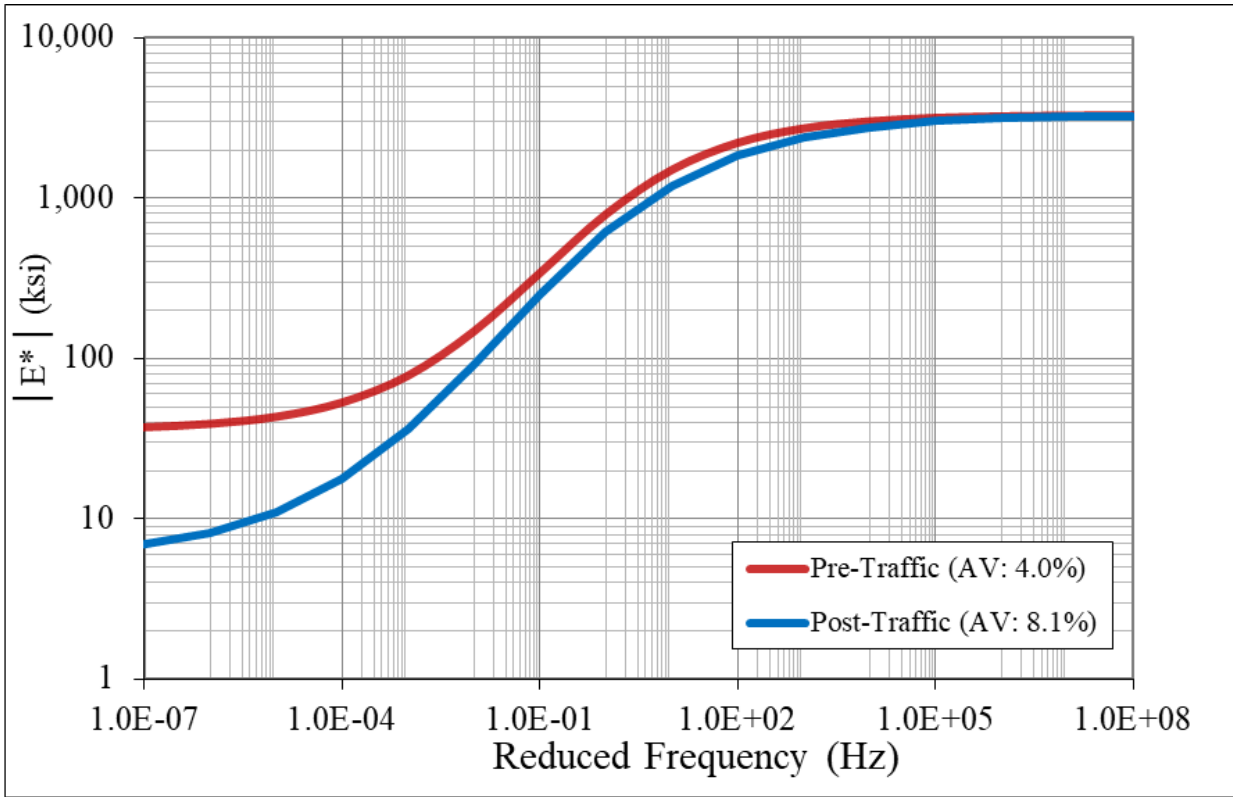


Figure 13. Dynamic Modulus Master Curves

The post-traffic dynamic modulus was about 750 ksi at a frequency of 2.47 Hz. This frequency represented the loading frequency at the pavement surface corresponding to CC7 trafficking speed of 2.5 mph at the National Airport Pavement Test Facility (NAPTF), assuming 55,000 pounds for the wheel load and 220 psi for the tire pressure (10). Similarly, the pre-traffic modulus was found to be 1100 ksi. The pre-traffic data showed higher modulus at all frequencies than the post-traffic data, which was expected for an asphalt mixture with lower air voids.

Table 7. Summary of Dynamic Modulus Test Results for P-401 Mixture (North Side)

Conditions		Specimen 1		Specimen 2		Specimen 3		Average Modulus (ksi)	COV (%)	Average	
Temperature (°F)	Frequency (Hz)	Modulus (ksi)	Phase Angle (°)	Modulus (ksi)	Phase Angle (°)	Modulus (ksi)	Phase Angle (°)			Phase Angle (°)	COV (%)
14	0.1	2547.2	7.9	2621.0	8.1	2800.7	7.8	2656.3	4.9	7.9	1.4
	0.5	2875.1	6.6	2957.2	6.7	3150.9	6.4	2994.4	4.7	6.5	1.7
	1	3007.9	6.0	3096.4	6.1	3294.0	5.9	3132.8	4.7	6.0	1.8
	5	3311.8	4.8	3401.9	5.0	3604.6	4.7	3439.4	4.4	4.8	2.7
	10	3429.1	4.4	3519.3	4.5	3721.7	4.2	3556.7	4.2	4.3	3.8
	25	3493.5	4.0	3664.7	4.0	3851.5	3.6	3669.9	4.9	3.8	6.3
39	0.1	1238.3	17.3	1139.7	18.6	1222.2	18.8	1200.1	4.4	18.2	4.7
	0.5	1596.9	14.1	1496.8	15.3	1629.5	15.1	1574.4	4.4	14.8	4.6
	1	1756.3	12.9	1662.9	14.1	1811.7	13.9	1743.6	4.3	13.6	4.6
	5	2146.0	10.5	2069.1	11.4	2248.7	11.1	2154.6	4.2	11.0	4.2
	10	2307.0	9.4	2248.2	10.4	2427.5	10.1	2327.6	3.9	10.0	5.3
	25	2516.3	8.2	2479.0	9.0	2666.8	8.7	2554.0	3.9	8.6	4.4
70	0.1	274.6	32.5	264.1	31.2	244.2	33.2	261.0	5.9	32.3	3.1
	0.5	456.1	29.4	440.0	28.7	421.8	30.5	439.3	3.9	29.5	3.0
	1	547.1	28.3	529.7	27.7	514.2	29.4	530.3	3.1	28.4	3.0
	5	847.6	23.5	824.0	23.2	821.5	24.7	831.0	1.7	23.8	3.1
	10	986.7	21.7	964.5	21.7	971.5	22.9	974.2	1.2	22.1	3.2
	25	1194.8	19.1	1177.0	19.2	1196.0	20.2	1189.3	0.9	19.5	3.0
99	0.1	66.3	31.1	61.7	28.6	58.7	30.0	62.3	6.1	29.9	4.2
	0.5	121.6	32.9	111.4	30.9	105.8	32.6	112.9	7.1	32.1	3.3
	1	150.0	34.8	139.9	32.5	132.0	34.4	140.6	6.4	33.9	3.6
	5	301.5	31.5	272.1	30.9	270.9	32.2	281.5	6.2	31.5	2.1
	10	385.1	30.7	352.2	30.3	352.0	31.6	363.1	5.2	30.9	2.2
	25	517.1	29.4	480.1	29.3	481.7	30.6	492.9	4.2	29.8	2.4
129	0.1	17.3	26.8	17.1	25.9	18.4	24.6	17.6	3.9	25.8	4.4
	0.5	29.2	31.5	29.2	30.5	29.3	29.4	29.2	0.2	30.5	3.4
	1	39.1	31.8	38.0	31.6	35.5	32.3	37.5	5.0	31.9	1.2
	5	97.8	28.0	94.0	28.2	91.3	28.8	94.4	3.4	28.3	1.4
	10	144.7	27.4	140.6	27.7	139.1	28.3	141.4	2.0	27.8	1.7
	25	210.7	29.8	209.6	29.8	208.6	30.7	209.6	0.5	30.1	1.8

4.2.1.3 Flow Number

The Flow Number tests were conducted at 126 °F with deviator stress and contact stress of 200 psi and 5 psi respectively. The tests were conducted on the dynamic modulus specimens for the north side and were continued until termination or 10,000 cycles, whichever came first. The termination was defined as reaching a microstrain level of 50,000. For the post-traffic cores, the FN was found to be 127. For comparison, the FN for pre-traffic test specimens was 262 (3).

4.2.1.4 High Temperature Indirect Tensile Strength (IDTH)

IDTH strength is calculated as shown in Equation 9:

$$IDT\ Strength = \frac{2P}{\pi dt} \quad \text{Equation 9}$$

where P is the maximum applied load (pounds), d is diameter of the specimen (inches), and t is thickness of the specimen (in). The average IDTH strength for the north and south sides was 61 psi and 31 psi, respectively. Load vs. displacement for the three test specimens are provided in figure 14. As expected, the north side test samples (higher PG) endured much higher load before failure than south side test samples (lower PG). Similar trend was also observed for the pre-traffic data (3).

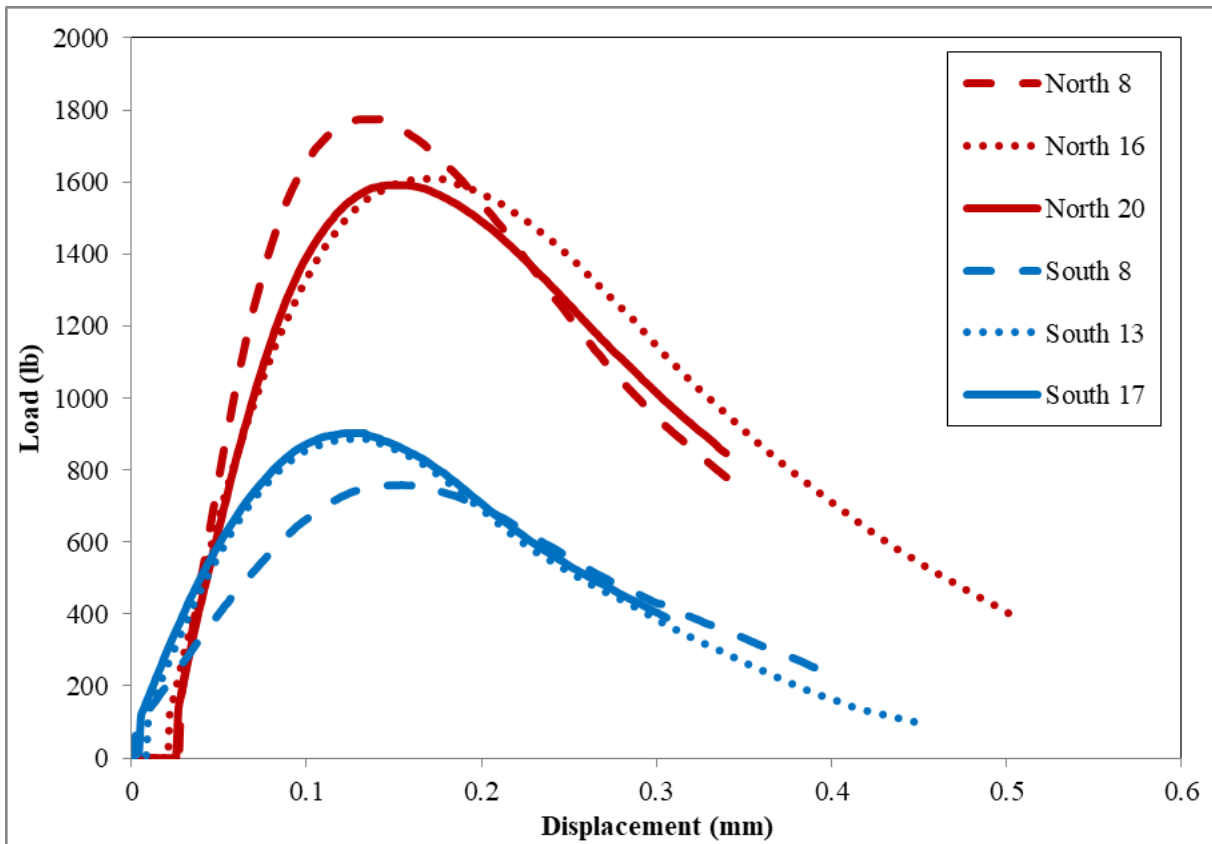


Figure 14. IDTH Load vs. Displacement Curves for North and South Sides

4.2.1.5 Tensile Strength Ratio

The tensile strength ratio (TSR) is defined as Equation 10.

$$TSR = \frac{S_{tm}}{S_{td}} \times 100 \quad \text{Equation 10}$$

where TSR is the tensile strength ratio (%), S_{tm} is the average tensile strength of the moisture-conditioned specimens (psi), and S_{td} is the average tensile strength of the dry specimens (psi). Table 8 shows the tensile strength test results. Although the north side tensile strength values were higher than the south side, the TSR value was 75% for both sides, which was acceptable as per P-401 specifications (8). Moderate stripping of the aggregates was observed in both the north and south side specimens with partial aggregate fractures as seen in figure 15.

Table 8. Summary of TSR Test Results

Replicate	North Side		South Side	
	Dry Tensile Strength (psi)	Wet Tensile Strength (psi)	Dry Tensile Strength (psi)	Wet Tensile Strength (psi)
#1	55.8	44.8	32.1	25.2
#2	43.7	34.2	35.4	23.5
#3	53.6	36.5	32.4	26.3
Average	51.0	38.5	33.3	25.0
TSR (%)	75		75	



(a) North Side



(b) South Side

Figure 15. TSR Specimens

4.2.2 ATDB Characterization Tests

4.2.2.1 Asphalt Pavement Analyzer

Six 3-inch height by 6 inch in diameter APA samples were tested at 100 psi and 250 psi for both the ATDB specimens. The APA tests were conducted at 147°F with the cyclic load applied at the rate of one cycle per second. The terminal rut depth of the specimens was set at 0.47 inch (12 mm) or 10,000 cycles, whichever comes first. The APA test results for the ATDB are provided in table 9 and figures 16 and 17. Rut depth at 25 cycles was arbitrarily chosen as a baseline to compare results between 100 and 250 psi.

Table 9. Summary of APA Test Results for ATDB

Wheel Location	Air Voids (%)	Rut Depth (mm) @ 25 cycles		
		Left	Center	Right
100 psi	21.9	1.04	0.77	0.90
250 psi	20.5	1.10	1.32	1.34

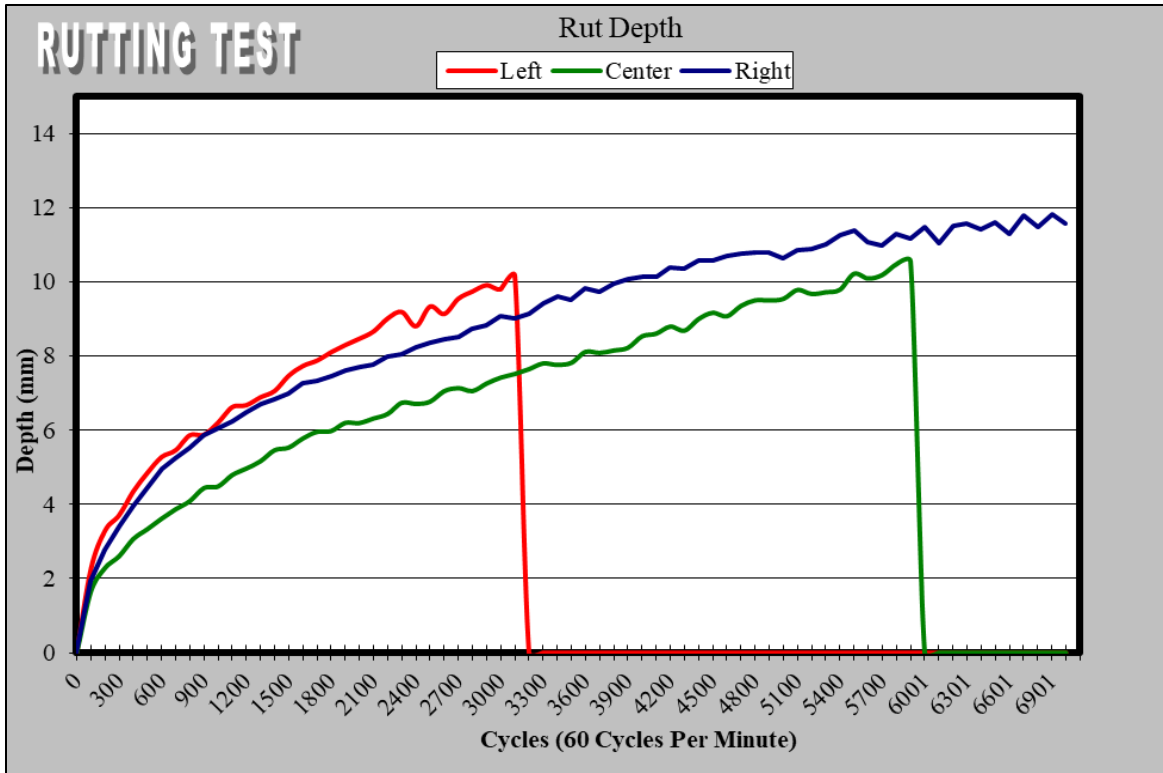


Figure 16. APA Test Results for ATDB at 100 psi and 147°F

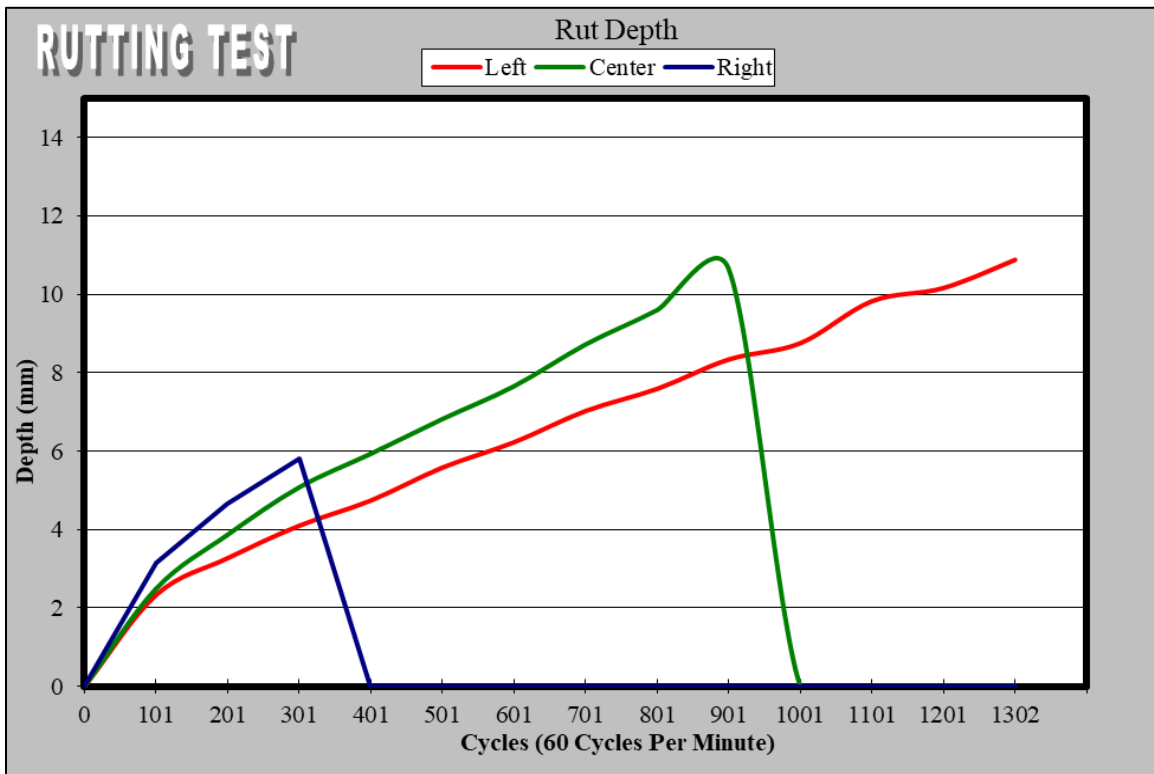


Figure 17. APA Test Results for ATDB at 250 psi and 147°F

4.2.2.2 Dynamic Modulus

Dynamic modulus test was conducted as per AASHTO TP79 “*Determining the Dynamic Modulus and Flow Number for Asphalt Mixtures Using the Asphalt Mixture Performance Tester*” for the ATDB cored specimens. Three specimens with a diameter of 4 inches and trimmed to the height of 6 inches were tested at four temperatures: 14, 39, 70, and 99°F using loading frequencies of 25, 10, 5, 1, 0.5, and 0.1 Hz. The modulus and phase angle at different temperatures and frequencies are presented in table 10. Figure 18 provides the master curves developed at a reference temperature of 70°F.

4.2.2.3 Falling Head Permeability Test

Table 11 shows the results of the falling head permeability test for both non-trafficked and trafficked areas. The coefficient of permeability for the non-trafficked area was 2.2 times higher than the trafficked area. As expected, the slab thickness and air voids were lower in the trafficked area.

Table 10. Summary of Dynamic Modulus Test Results for Drainable Base

Conditions		Specimen 1		Specimen 2		Specimen 3		Average Modulus (ksi)	COV (%)	Average	
Temperature (°F)	Frequency (Hz)	Modulus (ksi)	Phase Angle (°)	Modulus (ksi)	Phase Angle (°)	Modulus (ksi)	Phase Angle (°)			Phase Angle (°)	COV (%)
14	0.1	1263.1	10.4	1167.6	8.9	1110.8	9.8	1180.5	6.5	9.7	0.8
	0.5	1464.3	8.5	1333.3	7.2	1286.2	8.0	1361.3	6.8	7.9	0.6
	1	1548.9	7.7	1402.5	6.6	1361.2	7.4	1437.5	6.9	7.3	0.6
	5	1732.3	6.0	1556.0	5.4	1523.5	6.0	1603.9	7.0	5.8	0.3
	10	1804.3	5.5	1617.5	4.9	1590.5	5.5	1670.7	7.0	5.3	0.3
	25	1902.5	4.7	1695.6	4.3	1676.2	4.8	1758.1	7.1	4.6	0.3
39	0.1	463.4	19.7	540.6	18.9	574.9	18.0	526.3	10.9	18.9	0.8
	0.5	622.2	16.5	722.1	15.7	749.1	15.1	697.8	9.6	15.7	0.7
	1	695.3	15.2	806.6	14.5	827.9	13.9	776.6	9.2	14.5	0.7
	5	880.1	12.4	1009.5	11.7	1025.3	11.3	971.6	8.2	11.8	0.6
	10	959.1	11.3	1098.4	10.7	1112.7	10.2	1056.7	8.0	10.7	0.5
	25	1068.3	9.9	1218.6	9.2	1227.3	8.9	1171.4	7.6	9.3	0.5
50	0.1	299.6	23.3	311.5	24.3	357.8	22.8	323.0	9.5	23.5	0.8
	0.5	418.6	20.4	447.4	21.1	497.3	19.8	454.5	8.8	20.4	0.7
	1	477.3	19.2	515.0	19.8	566.7	18.7	519.7	8.6	19.2	0.6
	5	646.0	15.9	698.1	16.3	759.6	15.3	701.2	8.1	15.8	0.5
	10	721.7	14.5	782.6	15.0	846.0	14.0	783.4	7.9	14.5	0.5
	25	826.9	12.7	898.8	13.1	966.7	12.2	897.4	7.8	12.7	0.4
70	0.1	125.3	28.2	111.0	29.2	147.9	28.0	128.1	14.5	28.5	0.6
	0.5	199.6	26.5	178.8	28.0	237.4	26.0	205.3	14.5	26.8	1.0
	1	237.1	25.9	214.1	27.6	282.2	25.4	244.5	14.2	26.3	1.2
	5	362.9	22.4	337.6	23.8	427.9	21.6	376.1	12.4	22.6	1.1
	10	427.7	20.8	403.5	22.2	503.6	20.1	444.9	11.7	21.0	1.0
	25	523.9	18.6	501.3	19.9	613.7	17.9	546.3	10.9	18.8	1.0
99	0.1	25.5	28.8	31.1	26.2	42.5	27.0	33.0	26.3	27.4	1.3
	0.5	45.5	30.3	53.2	28.3	71.7	28.2	56.8	23.7	28.9	1.2
	1	53.6	33.2	63.0	30.8	86.2	29.3	67.6	24.7	31.1	2.0
	5	113.9	29.3	127.3	27.8	163.0	27.0	134.7	18.8	28.0	1.2
	10	154.0	28.2	169.7	26.9	211.2	26.0	178.3	16.6	27.1	1.1
	25	210.7	27.6	225.8	26.9	279.1	25.4	238.5	15.0	26.6	1.1

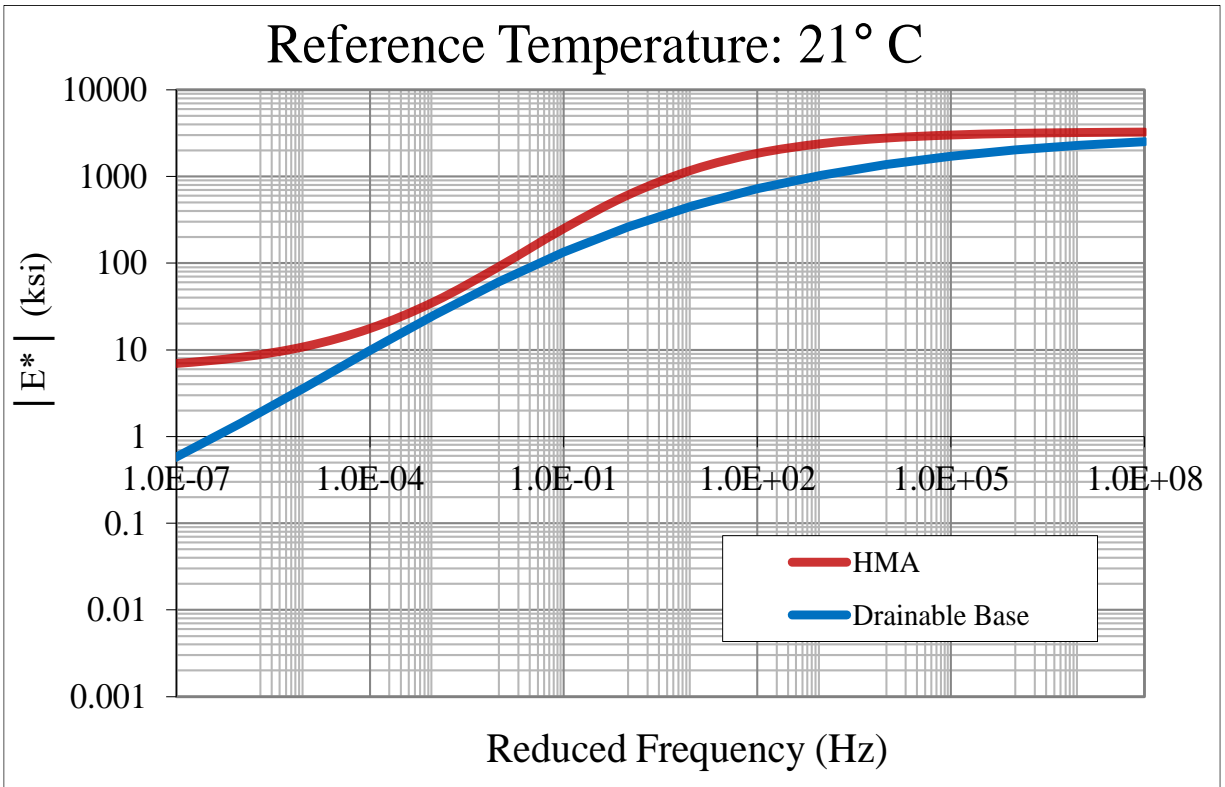


Figure 18. Comparison of Dynamic Modulus Master Curves for P-401 and ATDB

Table 11. Results of Falling Head Permeability Test on ATDB

Test Section	Slab Thickness (in.)	Air Voids (%)	Time (minutes)	Coefficient of Permeability (feet/day)
LFS-6N (NT-1)	7.5	21.2	0.4295	1,858
LFS-6N (NT-2)			0.3628	2,200
LFS-6N (NT-3)			0.3927	2,032
LFS-6N (NT-4)			0.3982	2,004
Average				2,024
LFS-6N (T-1)	6.6	17.7	0.6772	1,179
LFS-6N (T-2)			0.8785	908
LFS-6N (T-3)			1.0002	798
LFS-6N (T-4)			0.9198	868
Average				938

(T-1), (T-2), (T-3), (T-4): trafficked material-replicate 1, 2, 3, and 4; respectively

(NT-1), (NT-2), (NT-3), (NT-4): non-trafficked material-replicate 1, 2, 3, and 4; respectively

4.3 OBSERVATIONS

The APA rut depths for the north side were slightly lower than the south side at both 100 and 250 psi pressures. Both north and south sides performed well as per the recommended criteria for satisfactory APA rutting performance. FN, IDTH, and tensile strength from the TSR test were significantly higher for the north side test specimens as compared to the south side due to the use of polymer modified binder (PG 76-22). The TSR value was found to be satisfactory for both north and south side test sections (TSR = 75%). The coefficient of permeability for the non-trafficked area was 2.2 times higher than the trafficked area.

5. P-209 AGGREGATE BASE AND P-154 SUBBASE MATERIAL

5.1 SAMPLE COLLECTION

Originally in 2017, bulk samples of P-209 aggregate base and P-154 granular subbase materials from CC7 post-traffic trenches (see figure 19 for an overall layout) were collected (see Appendix A, *CC7 Post-Traffic Trenching and Test Plan*). However, the excavation method (mechanical excavator) and sampled P-209 aggregate base material was later discovered it had not captured the field P-209 material gradation. Therefore, manual sampling of P-209 material was conducted later in 2018, at the locations indicated in figure 20. Appendix A also includes details of this 2nd round of P-209 sample collection (*NAPTF CC7 Post-Traffic P-209 Sampling, Evaluation, and Testing Plan*).

5.1.1 Triaxial Specimen Preparation

Field measured values from construction phase were used to determine the target moisture-density condition for the laboratory compaction of P-154 triaxial specimens. The P-154 subbase material specimens were compacted to a target dry density of 134 pcf with 4.5% moisture content. This target dry density reasonably matched the maximum density from laboratory compaction curves. The specimens tested in the IPC Global system (i.e., 4-inch diameter by 8-inch height) were prepared following an impact compaction method, which consisted of repeatedly dropping a weight from a controlled height to impart dynamic energy on the sample (*II*). The P-154 specimens tested in the large MTS triaxial equipment (i.e., 6-inch diameter by 12-inch height) were compacted using a vibratory hammer. Regardless of compaction method, the density during compaction was controlled by measuring the height achieved for each lift of material.

Different from P-154 triaxial specimens, the target moisture-density condition for compaction of P-209 triaxial specimens was obtained from the laboratory compaction curve. The P-209 material specimens were compacted to the maximum dry density of 155.8 pcf with 4.1% moisture content (1% dry of optimum) using a vibratory hammer. Once mounted on the triaxial pedestal, specimens were covered with a latex membrane to isolate the material from the confining media per AASHTO T307.

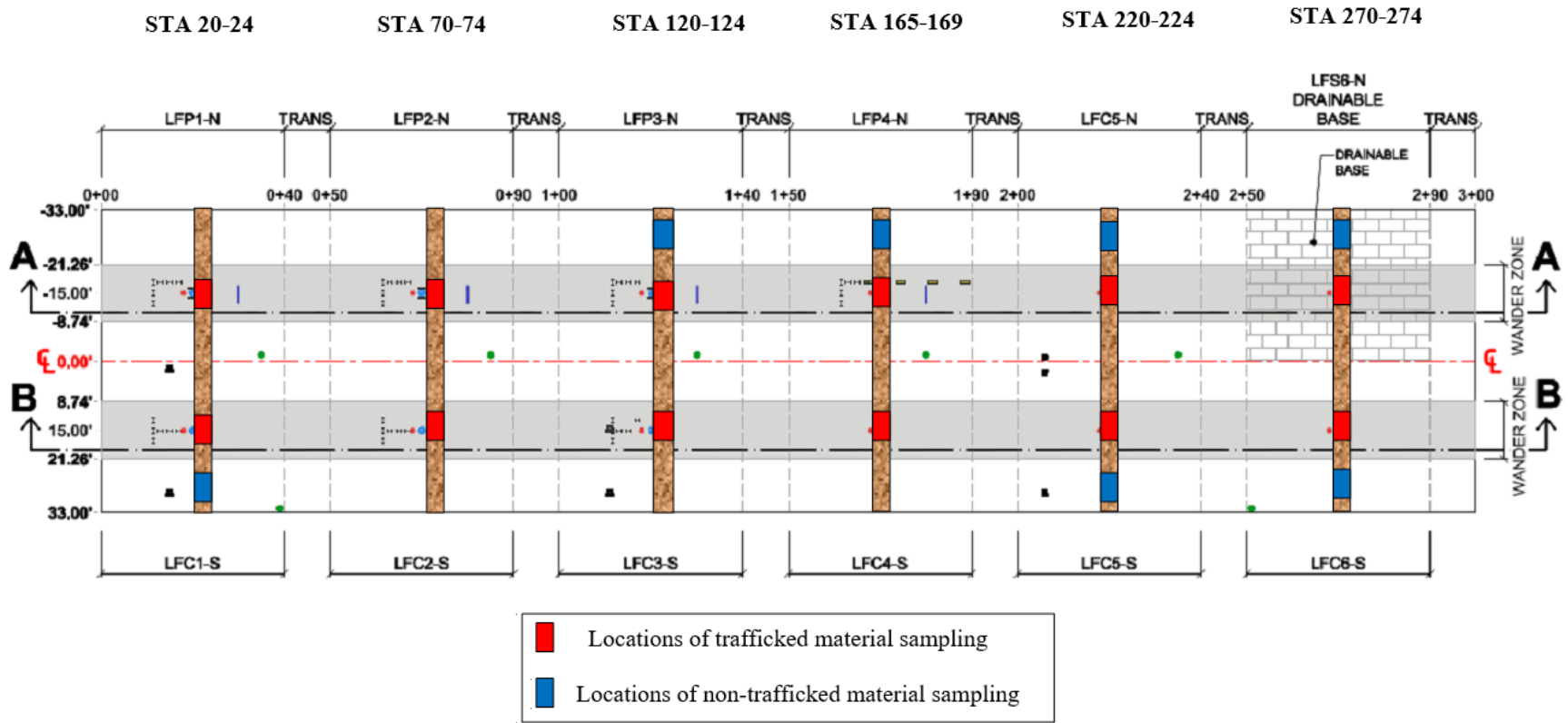


Figure 19. CC7 Trenching and Sampling Layout, 2017

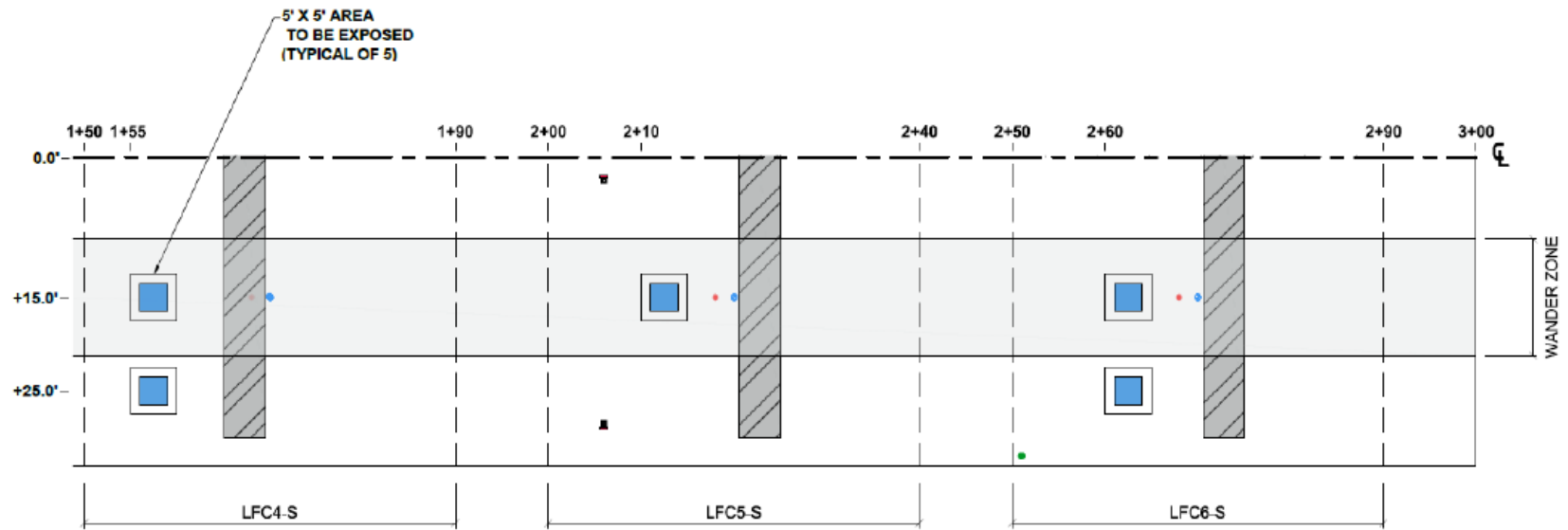


Figure 20. CC7 Locations for Additional P-209 Sampling, 2018

5.2 TEST RESULTS

5.2.1 Grain Size Distribution

Grain Size Distribution (GSD) was conducted following ASTM C117 and C136 standards. Eighteen and fifteen GSD tests were performed on bulk samples of P-154 and P-209 material, respectively.

5.2.1.1 P-209 Base Material in Overload Test Sections (South Side)

All CC7 south test sections had the same P-209 base layer thickness. Details can be found in the traffic test report (3). The P-209 GSD test results for sections LFC4-S, LFC5-S, and LFC6-S, are Summarized in table 12. Figure 21 shows the GSD test results of trafficked and non-trafficked materials from LFC4-S and LFC6-S, and trafficked materials from LFC5-S. No evidence of GSD changes as consequence of wheel/gear load changes was observed. The GSD curves of trafficked materials are bounded by the non-trafficked materials. In figure 22, the three GSD replicates in each group of material were averaged and plotted to further investigate the possible effects of varying traffic loads. Considering that the overload sequences followed increasing wheel load and decreasing gear load from west to east, no effect of wheel/gear load on the average GSD curves was shown. Figure 22 also shows higher content of sand and fines for trafficked materials than non-trafficked in LFC4-S, which was most likely due to either aggregate breakage during trafficking or inherent material variability. However, the opposite was observed for LFC6-S when comparing the two conditions. Non-trafficked materials had more medium to fine gravel, and sand content than trafficked materials, which should be attributed to material variability alone.

Table 12. CC7 Post-Traffic GSD of P-209 Base, South Side

Sample	Percent Finer						
	1.5"	1"	3/4"	#4	#30	#40	#200
Mesh	37.5	25.0	19.0	4.75	0.60	0.42	0.08
Sieve Opening (mm)							
LFC4-S (T-1)	100	93.8	76.6	34.9	14.6	13.3	9.2
LFC4-S (T-2)	100	93.7	77.7	35.1	14.3	13.0	8.8
LFC4-S (T-3)	100	92.6	72.2	32.8	13.3	12.1	8.2
LFC5-S (T-1)	100	93.2	77.2	39.1	16.5	14.9	9.8
LFC5-S (T-2)	100	88.8	69.0	29.0	13.1	12.0	8.0
LFC5-S (T-3)	100	89.3	68.0	29.6	13.4	12.2	8.2
LFC6-S (T-1)	100	93.8	76.0	33.4	12.3	11.9	9.7
LFC6-S (T-2)	100	94.8	78.8	39.3	16.2	15.1	10.0
LFC6-S (T-3)	100	92.4	78.3	37.6	15.6	14.1	9.6
LFC4-S (NT-1)	100	95.9	83.4	39.4	14.2	12.7	8.6
LFC4-S (NT-2)	100	93.0	75.9	29.5	11.5	10.5	7.3
LFC4-S (NT-3)	100	92.5	71.2	25.5	10.6	9.7	6.8
LFC6-S (NT-1)	100	95.8	83.8	46.2	15.8	14.7	9.4
LFC6-S (NT-2)	100	93.8	82.2	41.0	14.6	13.0	8.8
LFC6-S (NT-3)	100	96.1	82.3	41.0	14.6	13.1	8.8

(T-1), (T-2), (T-3): trafficked material-replicate 1, 2, and 3; respectively

(NT-1), (NT-2), (NT-3): non-trafficked material-replicate 1, 2, and 3; respectively

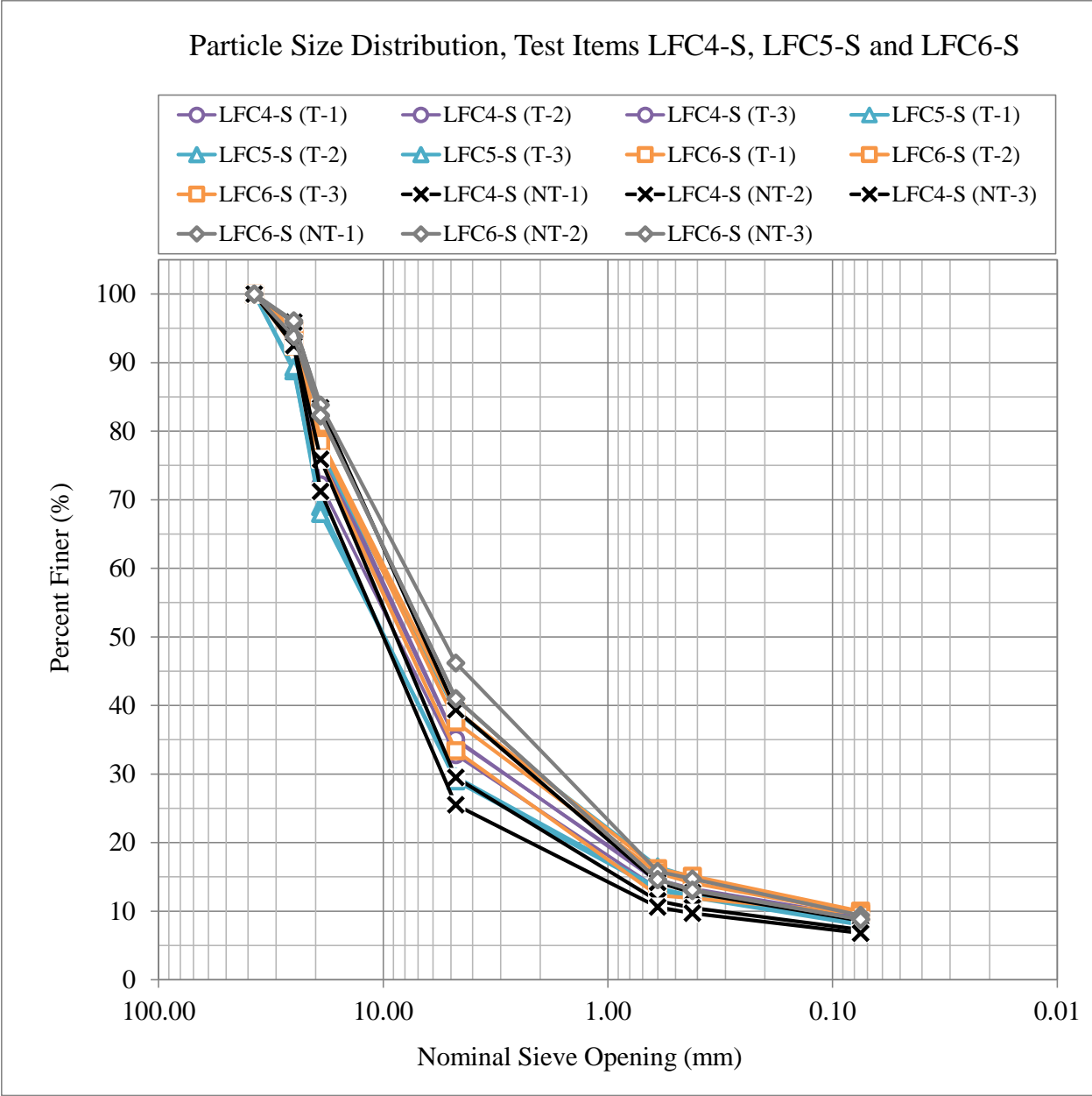


Figure 21. Post-Traffic GSD of P-209 Base from LFC4-S, LFC5-S, and LFC6-S, South Side

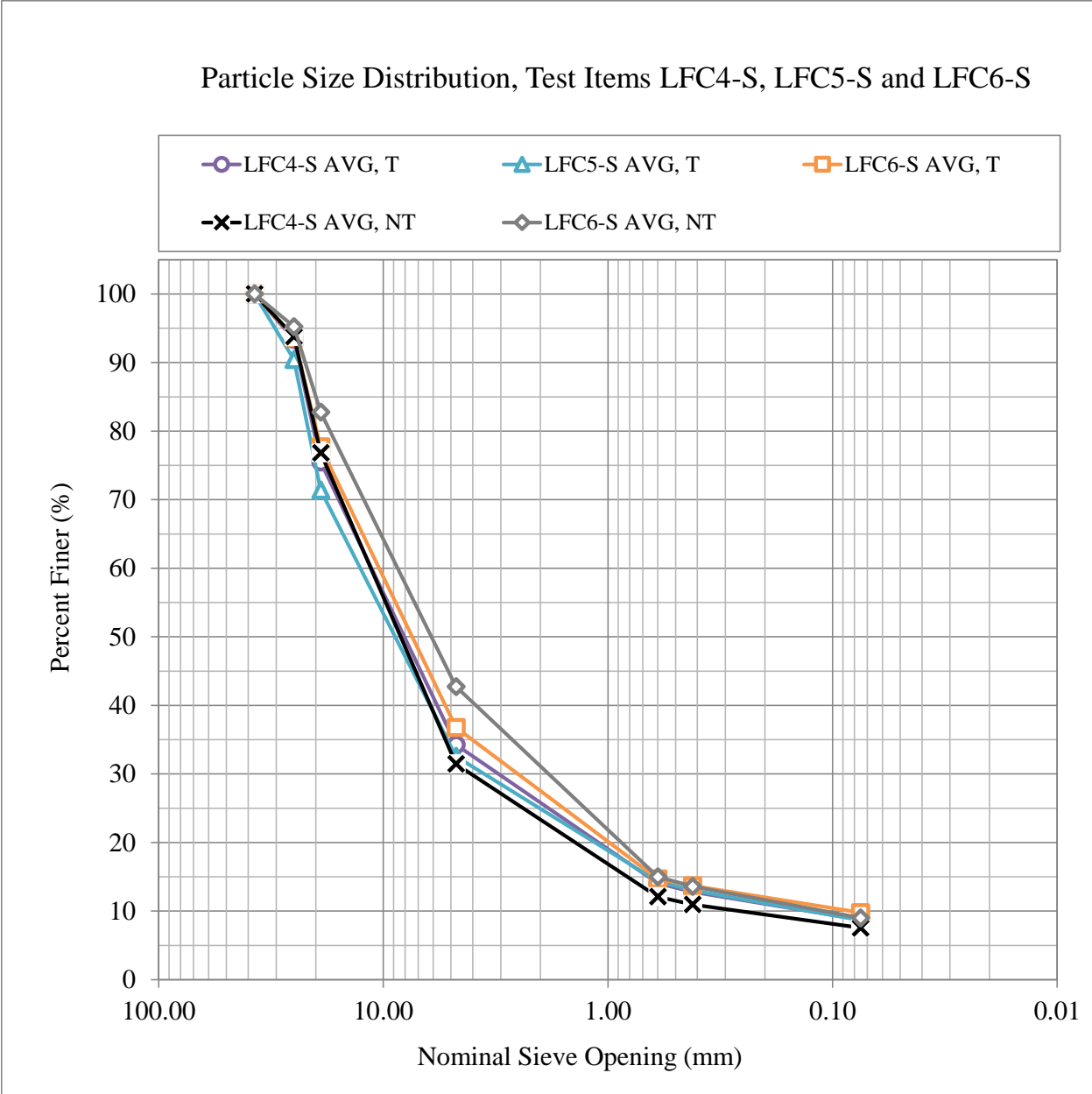


Figure 22. Post-Traffic Average GSD of P-209 Base from LFC4-S, LFC5-S, and LFC6-S, South Side

The relationship between grain size distribution and the mechanical behavior (i.e., shear strength and resilient properties) of aggregate base granular materials has been investigated by many researchers. Vallejo stated that in sand-gravel mixtures, the material strength is dominated by frictional resistance between gravel particles when the gravel content is greater than 70% of the mixture in weight (12). Also, it was reported that in mixtures with less than 49% gravel content, gravel particles have no control over shear strength. Xiao et al. proposed the gravel-to-sand (G/S) ratio as a link between mechanical behavior and GSD of the mixture. Xiao et al. postulated the existence of an optimal G/S ratio of about 1.5 that maximizes the shear strength behavior of aggregate mixtures used by Minnesota Department of Transportation (13). To further investigate

possible effects of overload magnitude and pattern in both the GSD and mechanical behavior of P-209 material, the G/S ratio observed in LFC4-S, LFC5-S, and LFC6-S is presented in figure 23.

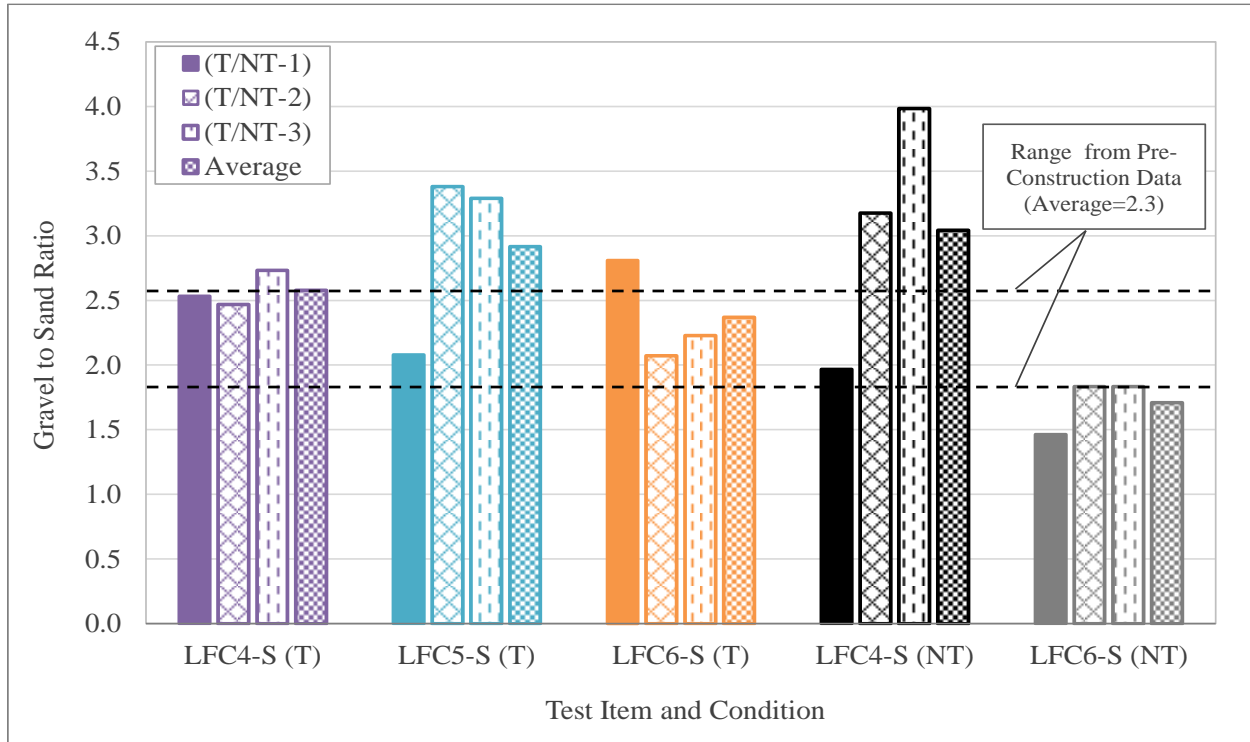


Figure 23. G/S Ratio of P-209 Base from LFC4-S, LFC5-S, and LFC6-S, South Side

There is no observable trend for the G/S ratio of trafficked materials that correlated to the varying wheel/gear load pattern. There is however an evident discrepancy between the G/S ratio for LFC4-S and LFC6-S non-trafficked materials. The black dashed lines indicate the range of G/S ratios obtained from pre-construction laboratory data. The pre-construction G/S ratio was found to be 2.3 in average (14). The average ratio in LFC4-S and LFC6-S non-trafficked materials fell above and below pre-construction data bounds, respectively. This is consistent with the GSD curves suggesting that the relatively high gravel content and low sand content observed for LFC4-S and LFC6-S non-trafficked materials can be directly attributed to material variability rather than particle breakage from traffic. In general, no solid evidence of possible effect of overload magnitude and pattern on the GSD of P-209 material was observed.

5.2.1.2 P-154 Subbase Material in Perpetual and Drainable Base Test Sections (North Side)

The P-154 subbase material was used in all CC7 north test sections. The full-scale traffic test was conducted at a constant wheel load of 55,000 pounds using 3 Dual Wheels in Tandem (3D) gear configuration. The relative effect of P-401 HMA thickness on the perpetual pavement performance was considered of particular interest when analyzing post-traffic GSD laboratory test results. The P-401 thickness of perpetual test sections LFP1-N, LFP2-N, LFP3-N, and LFP4-N was 15 inches, 12 inches, 10 inches, and 8 inches, respectively. GSD test results of P-154 material from perpetual test sections are presented in table 13. Gradation curves of trafficked P-154 materials are shown in figure 24. No significant changes in #200 sieve were observed among trafficked materials when

non-trafficked materials from LFP4-N was considered as the baseline. Materials finer than sieves #10 and #40 did increase for trafficked LFP3-N and LFP4-N, which have the thinner P-401 surface layers among all perpetual test sections. Even if non-trafficked materials from either LFP3-N or LFC5-N were considered as the baseline for comparison, the results showed that materials finer than sieves #10 and #40 in trafficked LFP3-N and LFP4-N increased (always for LFP3-N) or at least remained the same (non-trafficked LFP3-N compared to trafficked LFP4-N).

In figures 25(a), 25(b), and 25(c), direct comparisons of the percent finer than sieve #200, #40, and #10 between perpetual test sections are presented, respectively. As seen from figure 25(a), regardless of the test section, the deviation of fines content in the P-154 trafficked materials from the non-trafficked condition baseline was negligible. However, in figures 25(b) and 25(c), a significantly higher percent finer than sieves #40 and #10, relative to both the non-trafficked condition baseline and the values in LFP1-N and LFP2-N, was observed in LFP3-N and LFP4-N. LFP1-N and LFP2-N (i.e., sections with HMA surface layer equal or thicker than 12 inches) showed that the values of percent finer than sieves #200, #40 and #10 were about or below the non-trafficked condition baseline. Figures 25(b) and 25(c) showed LFP3-N with the most significant shift in percent finer compared to either the non-trafficked baseline condition or the values observed in LFP1-N and LFP2-N. Although the HMA surface layer in LFP4-N was 2 inches thinner, traffic test stopped after approximately 18,000 vehicle passes compared to LFP3-N where trafficking lasted over 35,000 vehicle passes.

Table 13. CC7 Post-Traffic GSD of P-154 Subbase from Perpetual Sections, North Side

Sample	Percent Finer								Overlying Pavement
	Mesh	1.5"	1"	3/4"	3/8"	#4	#10	#40	
Sieve Opening (mm)	38.1	25.4	19.0	9.51	4.76	2.00	0.420	0.074	
LFP1-N (T)	100	100	100	99.9	92.9	53.2	22.1	7.8	15" P-401
LFP2-N (T)	100	100	100	99.9	94.7	53.7	22.4	7.6	12" P-401
LFP3-N (T)	100	100	100	100	99.8	62.0	25.7	6.6	10" P-401
LFP3-N (NT)	100	100	100	100	99.7	60.0	24.7	6.1	10" P-401
LFP4-N (T)	100	100	100	100	99.7	60.6	24.4	7.4	8" P-401
LFP4-N (NT)	100	100	100	99.9	98.6	56.8	23.0	7.1	8" P-401

(T) trafficked material

(NT) non-trafficked material

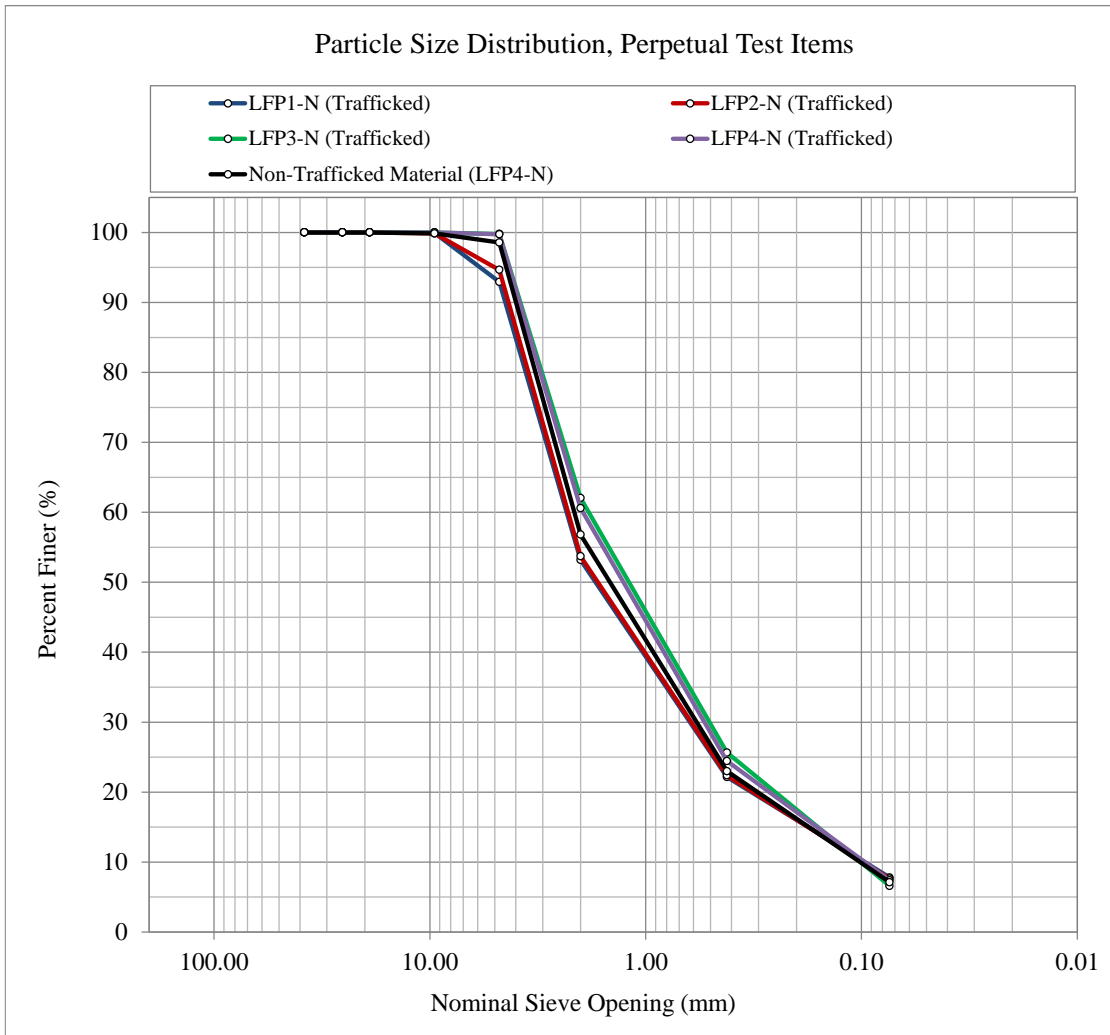
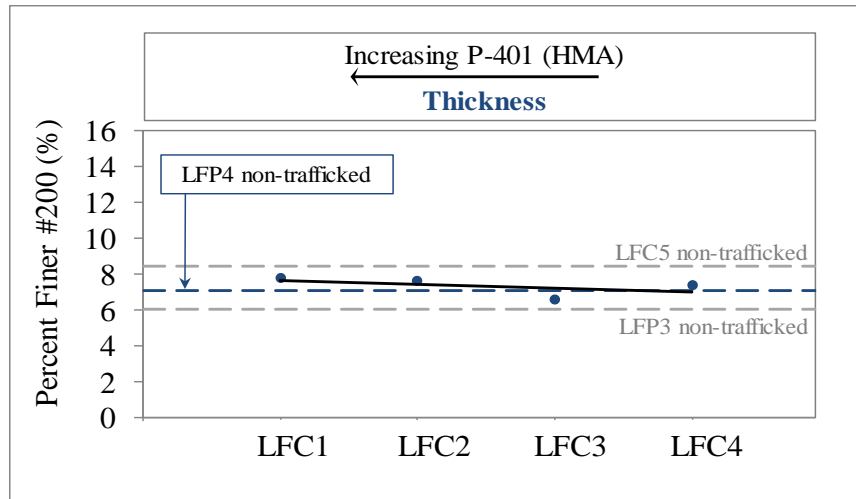
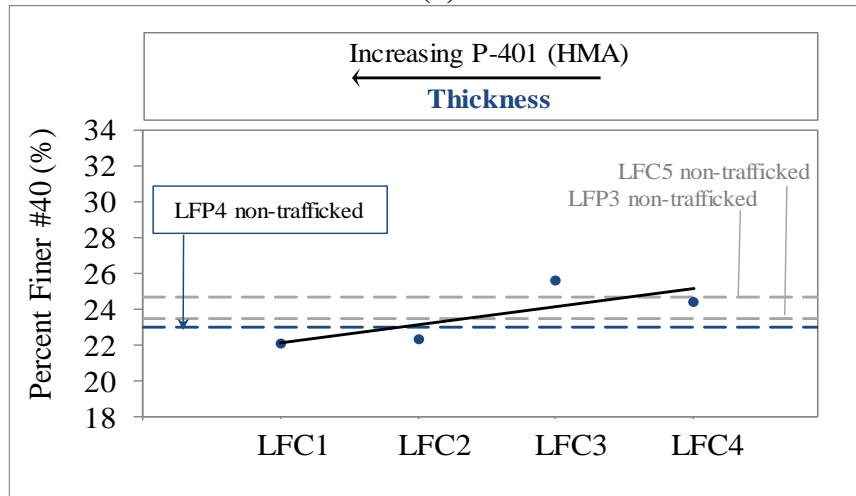


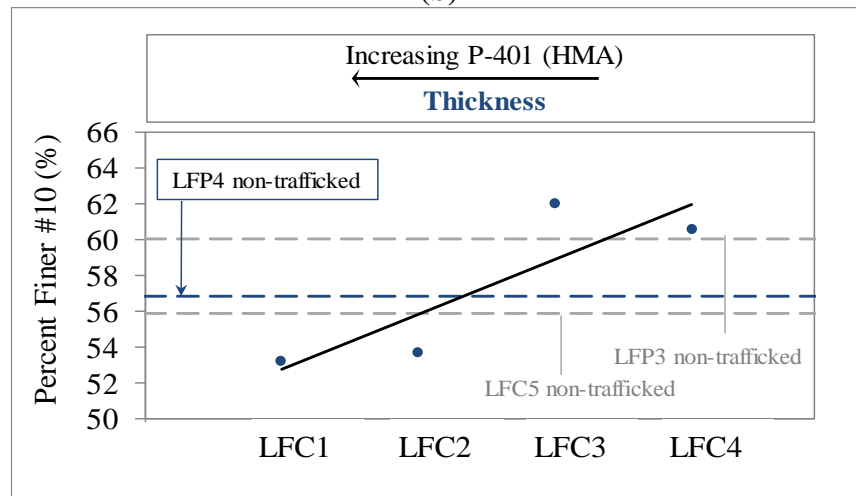
Figure 24. Post-Traffic GSD of P-154 Subbase from Perpetual Sections, North Side



(a)



(b)



(c)

Figure 25. Difference in GSD of P-154 Subbase Material among Perpetual Test Sections, North Side: (a) Percent Finer #200, (b) Percent Finer #40, (c) Percent Finer #10

GSD test results of P-154 material from ATDB test sections on the north side are presented in table 14 and figure 26 for LFC5-N and LFS6-N under both trafficked and non-trafficked conditions. No solid evidence of changes in gradation as a result of traffic was observed.

Table 14. CC7 Post-Traffic GSD of P-154 Material Drainable Base, North Side

Sample	Percent Finer								Overlying Pavement
	1.5"	1"	3/4"	3/8"	#4	#10	#40	#200	
Mesh	38.1	25.4	19.0	9.51	4.76	2.00	0.420	0.074	
Sieve Opening (mm)									
LFC5-N (T)	100	100	100	100	94.2	53.6	22.5	8.1	5" P-401 on 8" P-209
LFC5-N (NT)	100	100	100	99.9	94.3	55.9	23.5	8.5	5" P-401 on 8" P-209
LFS6-N (T)	100	100	100	100	92.6	51.3	19.8	5.7	5" P-401 on 8" ATDB
LFS6-N (NT)	100	100	100	99.7	97.6	59.4	23.9	8.0	5" P-401 on 8" ATDB

(T) trafficked material

(NT) non-trafficked material

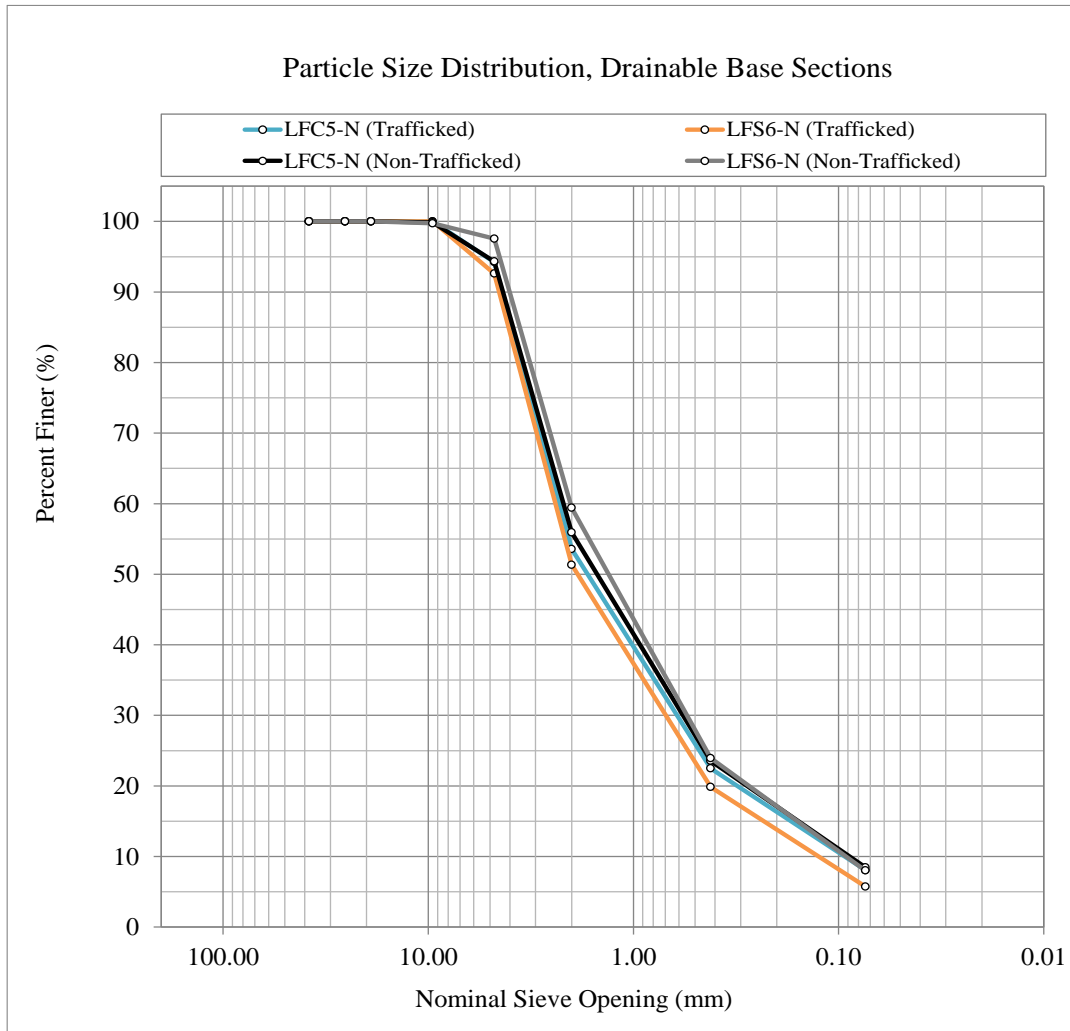


Figure 26. Post-Traffic GSD of P-154 Subbase Material from Drainable Base Test Sections, North Side

The amount of compaction energy imparted by traffic can be associated to aggregate breakage. LFC5-N and LFC6-N were subjected to 23,364 vehicle passes, whereas, the perpetual test sections (LFP1-N to LFP4-N) were subjected to more than 27,000 vehicle passes. Moreover, LFC5-N had an 8-in P-209 layer and LFC6-N had an 8-in ATDB layer which introduced another factor to be accounted for. Thus, the energy level imparted by full-scale traffic to P-154 material in LFC5-N and LFC6-N did not necessarily compare to that in perpetual test sections.

The changes in gradation observed in perpetual test sections are compatible with particle breakage under the attrition or abrasion mechanism. Figure 27 shows the types of aggregate breakage (15). Attrition or abrasion in unbound material particles increase the potential for loss of particle angularity which in turn leads to a reduction in friction angle. Although a correlation existed between compaction energy imparted to P-154 material by full-scale traffic (considering level of protection/cross section and vehicle passes applied to each test section) and characteristics of the GSD curve, additional test replicates are recommended for future laboratory testing programs of similar nature to rule out potential effects of material variability.

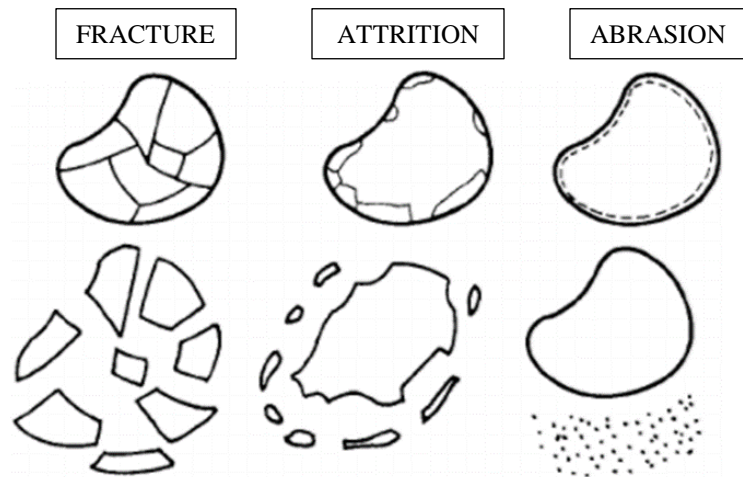


Figure 27. Types of Aggregate Breakage (15)

5.2.1.3 P-154 Subbase Material in Overload Test Sections (South Side)

All CC7 south test sections had the same P-154 subbase layer thickness. Details on the overload test can be found in referenced literature (3). In this section, the P-154 GSD test results of the overload test sections are presented. In figures 28 and 29, the GSD test results are plotted for LFC1-S, LFC2-S and LFC3-S (i.e., ACN/PCN test sections), and LFC4-S, LFC5-S and LFC6-S (i.e., CDF test sections), respectively. In both figures, considering the non-trafficked LFC1-S material as the baseline, higher fines content (i.e., percent finer than sieve #200) was observed for all the trafficked materials. Table 15 summarizes the GSD results.

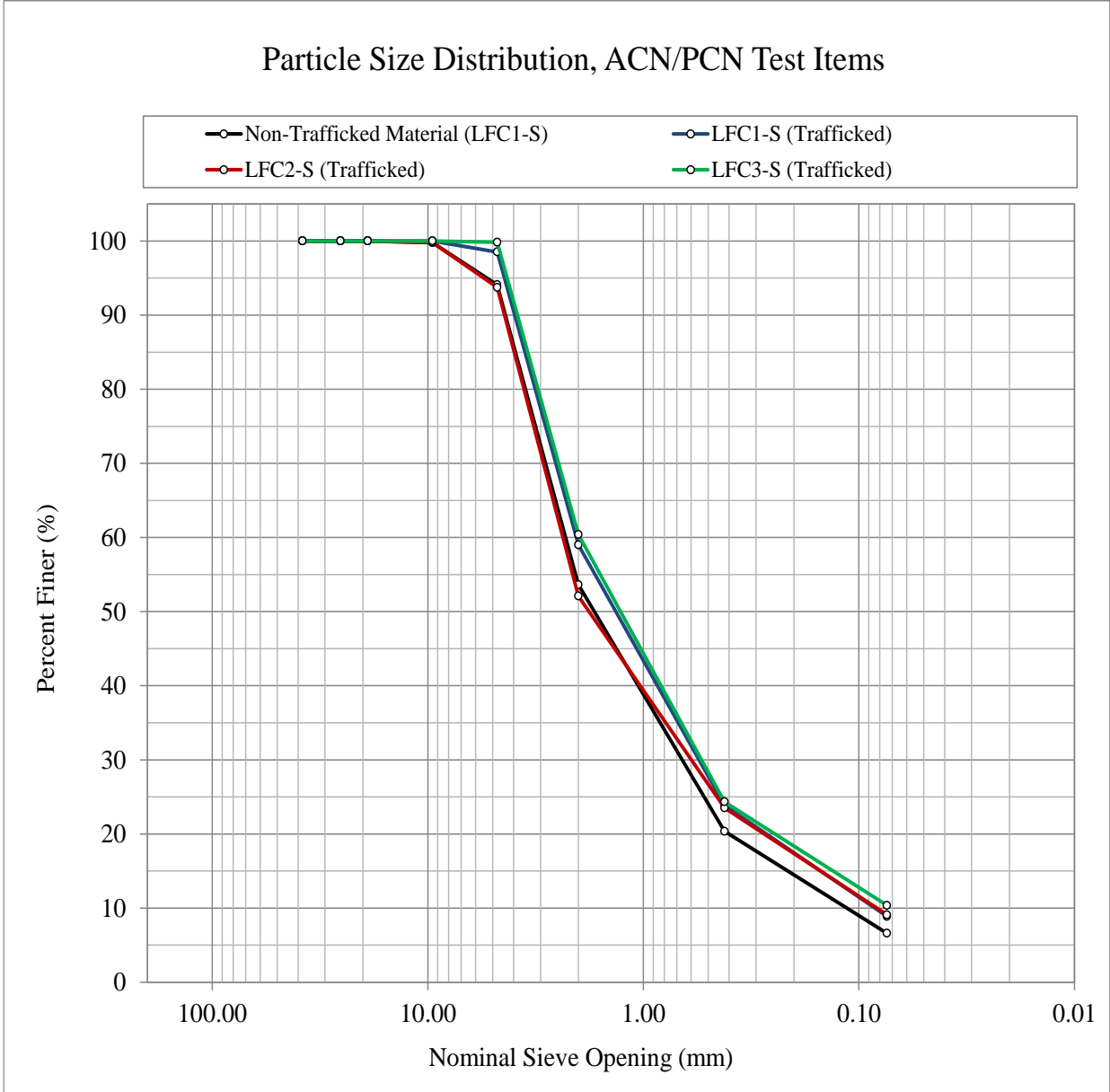


Figure 28. Post-Traffic GSD of P-154 Subbase Material from LFC1-S, LFC2-S, and LFC3-S Test sections, South Side

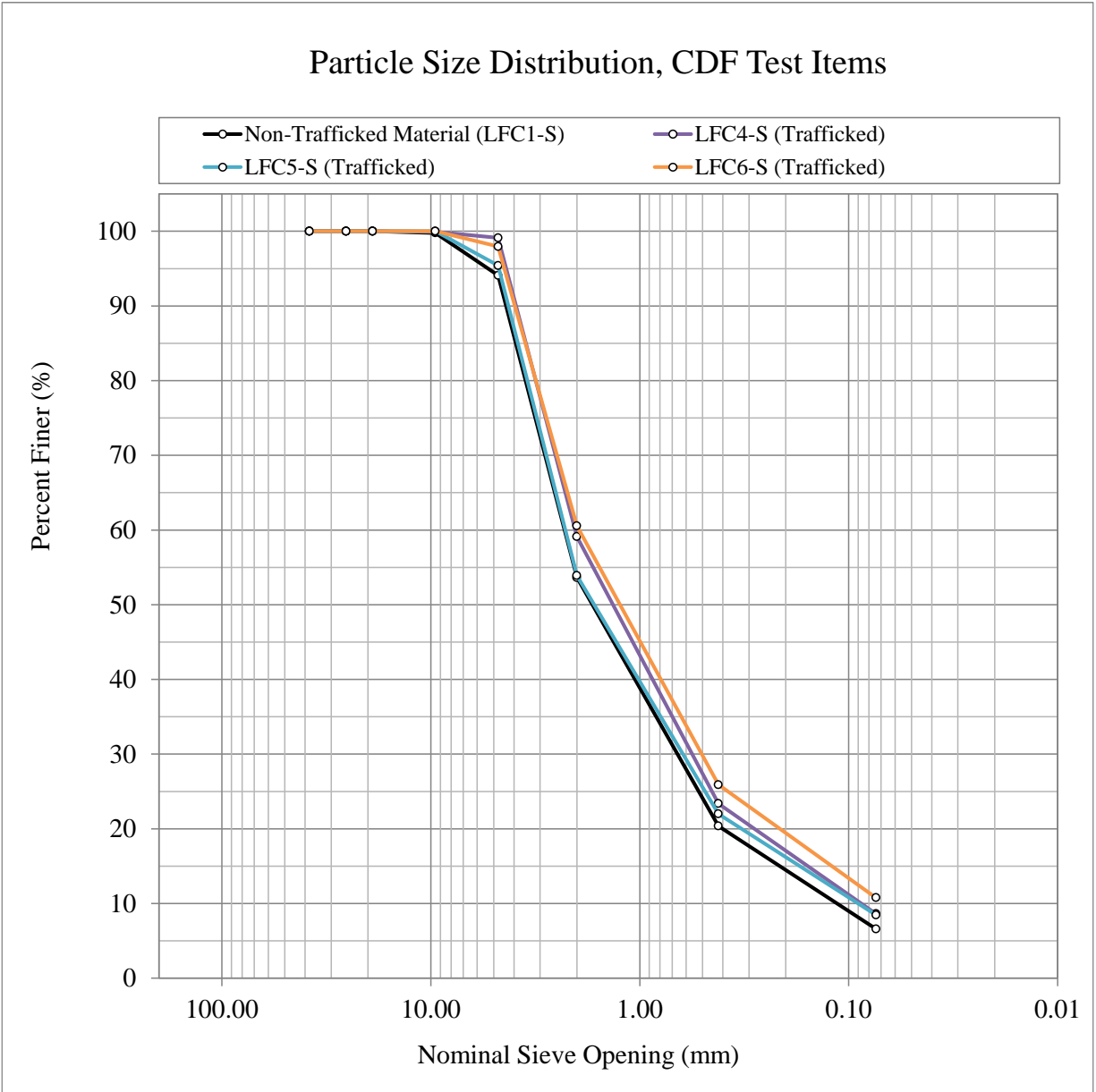


Figure 29. Post-Traffic GSD of P-154 Subbase Material from LFC4-S, LFC5-S, and LFC6-S Test Sections, South Side

Table 15. CC7 Post-Traffic GSD of P-154 Subbase, South Side

Sample	Percent Finer							
	1.5"	1"	3/4"	3/8"	#4	#10	#40	#200
Mesh	38.1	25.4	19.0	9.51	4.76	2.00	0.420	0.074
Sieve Opening (mm)								
LFC1-S (T)	100	100	100	100	98.5	59.0	23.9	8.9
LFC1-S (NT)	100	100	100	99.8	94.1	53.6	20.4	6.6
LFC2-S (T)	100	100	100	99.8	93.7	52.1	23.5	9.1
LFC3-S (T)	100	100	100	100	99.8	60.4	24.3	10.4
LFC4-S (T)	100	100	100	99.9	99.1	59.1	23.4	8.6
LFC5-S (T)	100	100	100	100	95.4	53.9	22.0	8.5
LFC5-S (NT)	100	100	100	100	92.8	50.5	18.4	5.8
LFC6-S (T)	100	100	100	100	98.0	60.5	25.9	10.8

(T) trafficked material

(NT) non-trafficked material

Particle abrasion is a particle breakage mechanism that can increase the fines content of unbound materials. In figure 30, a direct comparison of post-traffic fines content in all of the overload test sections is presented. As can be seen, increasing gear load coincided with increasing fines content for test sections LFC1-S, LFC2-S, and LFC3-S; whereas increasing wheel load coincided with increasing fines content for test sections LFC4-S, LFC5-S, and LFC6-S. These trends are consistent with the accumulation of permanent deformation observed during full-scale traffic testing. As observed in figure 31, increasing accumulation of permanent deformation corresponded to increasing fines content for both test section groups: LFC1-S to LFC3-S and LFC4-S to LFC6-S. Similar trends were also observed and reported from responses captured by CC7 instrumentation (3). It is known that in the case of abrasion, particle roundness tends to increase leading to a reduction in the friction angle.

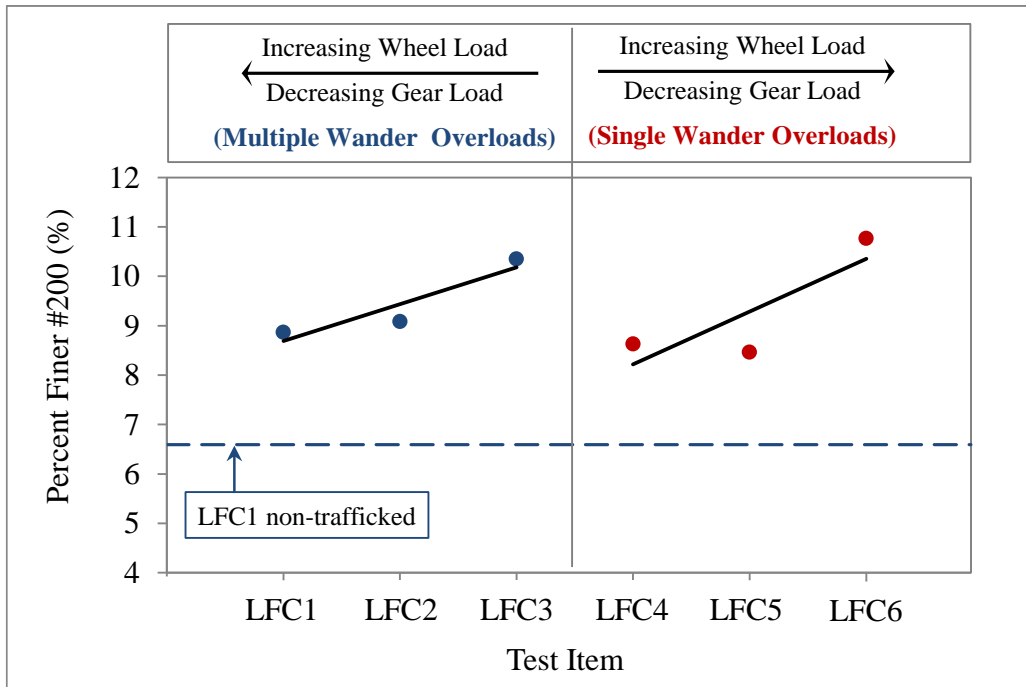


Figure 30. Comparison of Post-Traffic Fines content in P-154 Subbase Material for all Overload Test Sections, South Side

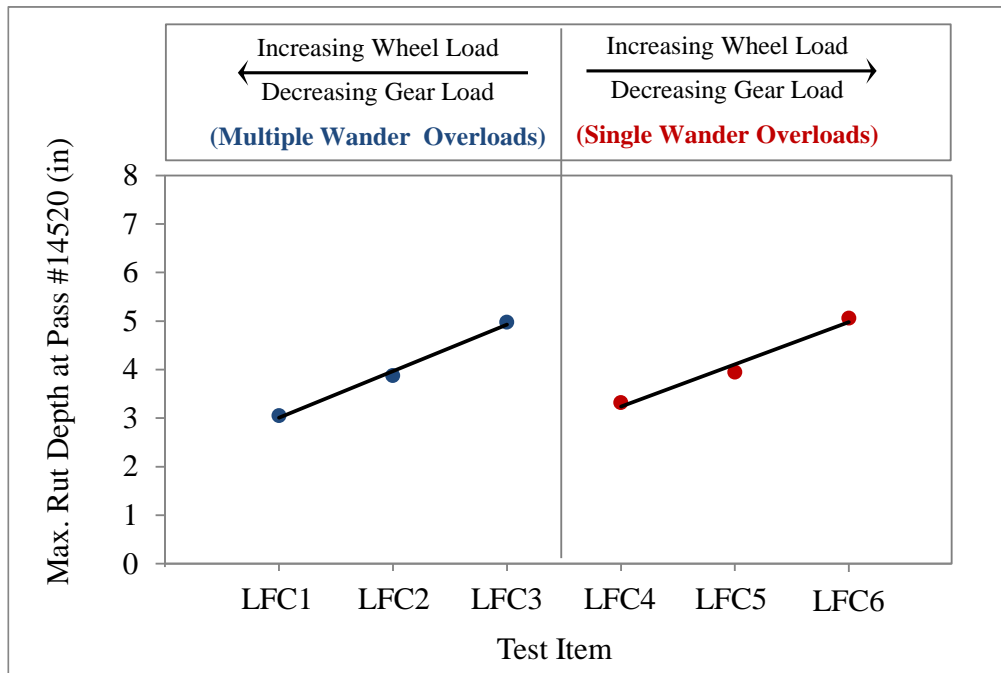


Figure 31. Comparison of Maximum Ruth Depth at Pass #14520 for all Overload Test Sections, South Side

5.2.2 Triaxial Test

Triaxial test was conducted on P-209 and P-154 material specimens in accordance with AASHTO T307 standard. The resilient modulus test was performed on all specimens followed by the quick shear test at different levels of confining pressure. A total of 52 triaxial tests were performed on reconstituted specimens of P-154 and P-209 materials as detailed in table 1. Most of the unbound materials tested were sampled from trafficked areas and only limited sampling was conducted in non-trafficked areas. Test reports of each single specimen are included in Appendix B.

The resilient modulus test data was fitted to the generalized enhanced version of the widely known universal model (16). The Mechanistic-Empirical Pavement Design Guide developed under the NCHRP 1-37A research project recommends the use of the universal model to characterize the non-linear stress dependency of resilient modulus. The model reads as follows:

$$M_R = k_1 \cdot p_a \left(\frac{\theta}{p_a} \right)^{k_2} \cdot \left(\frac{\tau_{oct}}{p_a} + 1 \right)^{k_3} \quad \text{Equation 11}$$

$$\theta = \sigma_1 + \sigma_2 + \sigma_3 \quad \text{Equation 12}$$

$$\tau_{oct} = \frac{1}{3} \cdot \sqrt{(\sigma_1 - \sigma_2)^2 + (\sigma_1 - \sigma_3)^2 + (\sigma_2 - \sigma_3)^2} \quad \text{Equation 13}$$

where; k_1 , k_2 , and k_3 are dimensionless regression constants, θ is the bulk stress, τ_{oct} is the octahedral shear stress, and p_a is atmospheric pressure. The constant k_1 should be a positive value and is proportional to the material Young's modulus. The value of k_2 should also be positive as any increase in the bulk stress term results in material stiffening or hardening. The value of k_3 is expected to be negative as any increase in the octahedral shear stress results in material softening. The quick shear data was used to determine shear strength parameters. In the following sections, the triaxial test results are presented and discussed by material type.

5.2.2.1 P-209 Base Material in Overload Test Sections (South Side)

A total of three resilient modulus replicates per sampled test section (i.e., LFC4-S, LFC5-S, and LFC6-S) and condition (i.e., trafficked and non-trafficked) were conducted for the P-209 aggregate base material. Upon completion of the resilient modulus portion, quick shear test was conducted using a different confining stress level for each replicate. As result, three sets of quick shear test data at confining pressures of 5, 10, and 15 psi were available to estimate shear strength parameters. These parameters were expected to provide information of any possible overload effects on material degradation due to full-scale traffic. Table 16 summarizes the resilient modulus and quick shear test results obtained for the sampled test sections. The moisture-density condition for each specimen is also indicated.

Table 16. Summary of Triaxial Test Results for P-209 Specimens

Specimen	Compaction Condition		Resilient Modulus					Quick Shear		
	Test Section	w (%)	ρ_{dry} (pcf)	M_R (psi)	k_1	k_2	k_3	S_e/S_y	R^2_{Adj}	σ_3 (psi)
LFC4-S (NT-1)	3.5	152.6	41,279	482	1.140	-0.010	0.232	0.94	5	75
LFC4-S (NT-2)	3.6	151.3	47,831	658	1.018	-0.010	0.131	0.98	11	132
LFC4-S (NT-3)	3.6	152.2	69,434	1,064	1.128	-0.467	0.064	1.00	15	177*
Average			52,848	734	1.095	-0.162	0.143	0.97		
LFC6-S (NT-1)	3.4	150.5	52,205	872	0.897	-0.010	0.212	0.95	5	57
LFC6-S (NT-2)	3.5	151.5	45,226	726	0.945	-0.040	0.158	0.97	10	102
LFC6-S (NT-3)	3.7	151.4	47,961	607	1.222	-0.362	0.189	0.96	15	140
Average			48,464	667	1.083	-0.201	0.174	0.96		
LFC5-S (T-1)	3.5	155.3	35,533	546	0.921	-0.010	0.259	0.92	5	56
LFC5-S (T-2)	3.5	154.2	45,802	878	0.812	-0.010	0.144	0.98	10	119
LFC5-S (T-3)	3.5	153.9	44,065	923	0.751	-0.010	0.274	0.91	15	145
Average			41,800	782	0.828	-0.010	0.226	0.94		
LFC6-S (T-1)	3.6	155.7	72,058	612	0.987	-0.010	0.142	0.98	5	87
LFC6-S (T-2)	3.5	150.7	41,654	975	1.131	-0.275	0.093	0.99	10	116
LFC6-S (T-3)	3.6	154.4	54,145	837	1.017	-0.182	0.098	0.99	15	164
Average			55,952	808	1.045	-0.155	0.111	0.98		
LFC4-S (T-1)	3.7	154.5	37,186	629	0.901	-0.010	0.235	0.93	5	81
LFC4-S (T-2)	3.6	151.6	46,406	738	1.026	-0.225	0.184	0.96	10	104
LFC4-S (T-3)	3.7	158.0	54,139	715	1.178	-0.316	0.147	0.97	15	155
Average			45,910	694	1.035	-0.184	0.189	0.96		

(T-1), (T-2), (T-3): trafficked material-replicate 1, 2, and 3; respectively

(NT-1), (NT-2), (NT-3): non-trafficked material-replicate 1, 2, and 3; respectively

*Test was stopped due to MTS system limit

It should be mentioned that the moisture content, $w\%$, corresponded to the final value measured upon completion of the test. Table 16 also shows the results of non-linear regression using the generalized enhanced version of the universal model (Equation 11). The k_1 , k_2 , and k_3 parameters are included in the table and are intended to be utilized in the future to characterize the non-linear behavior of P-209 material at different states of stress. Along with the regression parameters, predicted resilient moduli, M_R , corresponding to a confining pressure, σ_3 , of 15 psi and a cyclic stress, S_{cyclic} , of 27 psi (12th sequence in the resilient modulus test) are included in table 16 as reference values. Also, the standard error ratio, S_e/S_y , and adjusted coefficient of determination, R^2_{adj} , are included to explain the goodness of fit. Finally, the confining pressure applied during the quick shear test and the corresponding measured maximum vertical stress, σ_{v-max} , are reported. The low S_e/S_y with corresponding high R^2_{adj} values observed in the table evidence the good fit of the resilient modulus test data to the generalized enhanced version of the universal model.

The results presented in table 16 indicate that considering the state of stress used in the moduli computation, the average predicted M_R ranged from 41,800 psi to 55,952 psi. This range was deemed reasonable and consistent with the material type in question. Similar to the GSD test results, no evidence of possible overload magnitude and pattern effects on the modulus was

observed. Also, possible effects of particle breakage due to traffic were not observed when comparing trafficked versus non-trafficked material in test sections LFC4-S and LFC6-S.

The strength parameters for the P-209 material in each test section were estimated using the data presented in table 16. Figure 32 shows an example of the Mohr-Coulomb failure envelope observed for trafficked LFC4-S P-209 material. The Mohr-Coulomb failure envelopes obtained for the remaining test items can be found in Appendix B. The estimates of cohesion and friction angle, ϕ , for P-209 material are summarized in table 17. The standard deviation between the results for cohesion and ϕ values were found to be 2.0 and 1.3, respectively. The discrepancy in cohesion and ϕ values for the test sections (both trafficked and non-trafficked) was found to be minimal and not correlated to overload traffic. From this perspective, the general observations from GSD and resilient modulus testing on the P-209 material were found to be consistent with shear strength parameters.

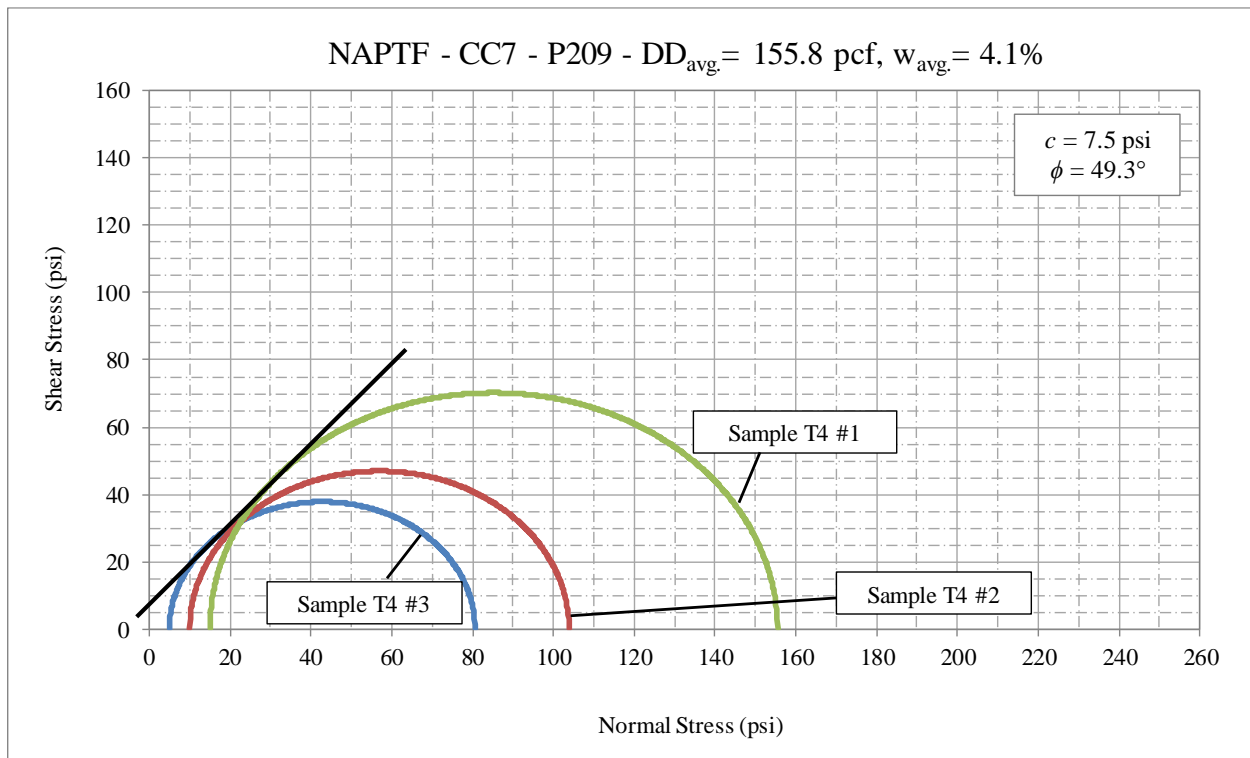


Figure 32. Mohr-Coulomb Envelope for the South Side P-209 Material, LFC4-S Test Item

Table 17. Summary of Strength Parameters for P-209 Specimens

Test Section	Strength Parameters	
	Cohesion (psi)	Friction Angle (°)
LFC4-S (NT)	6.0	52.6
LFC6-S (NT)	4.0	50.2
LFC4-S (T)	7.5	49.3
LFC5-S (T)	5.0	50.0
LFC6-S (T)	9.0	49.4
Average	6.3	50.3

(T) trafficked material

(NT) non-trafficked material

The average friction angle for P-209 material was found to be 50.3°. This value was higher than the average value of 47.4° obtained for P-154 samples prepared and tested under the same condition (i.e., sample size, compaction, and testing system). A friction angle of 60.8° at similar moisture-density conditions was reported during CC1 at the NAPTF database (14). However, the average gravel to sand ratio, G/S, of P-209 material used in CC1 was found to be 1.3 whereas for CC7 it was 2.3 (figure 23). As mentioned in previous sections, the literature reports the G/S ratio as a GSD-related parameter controlling the mechanical behavior in aggregate mixtures (12, 13, and 17). In figure 33, G/S ratios for CC1 and CC7 materials (i.e., P-209 and P-154) are plotted with their corresponding average friction angle values. At G/S=2.3 for CC7 P-209 material, the voids between gravel particles were only partially occupied by sand grains and the porosity was not ideal, which resulted in an unstable mixture. At lower G/S ratios such as that of CC1 P-209 material, the porosity of the mixture was expected to be minimal and shear strength expected to be optimal. For aggregate mixtures with very low G/S values such as CC1 and CC7 P-154 material, a matrix of sand grains had control over the shear strength of the mixture (12, 13, and 17).

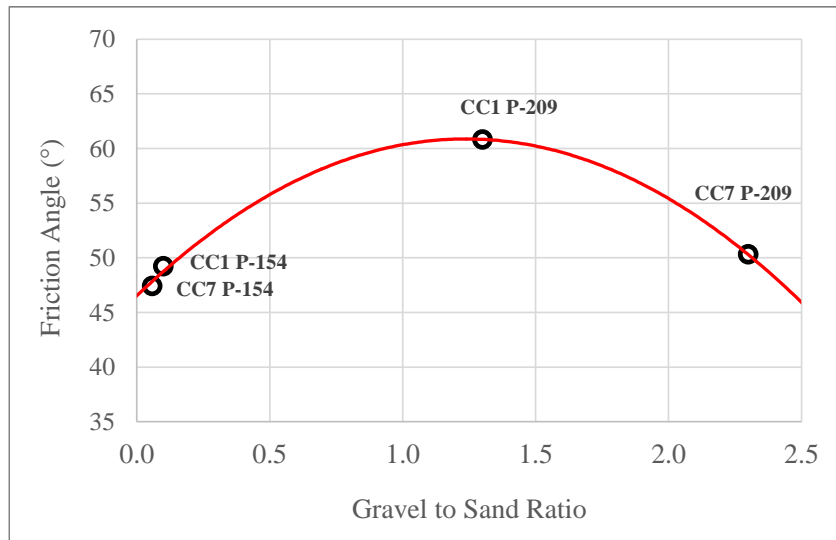


Figure 33. Relationship between G/S and Friction Angle for CC1 and CC7 Materials

5.2.2.2 P-154 Subbase Material in Perpetual Test Sections (North Side)

Considering that thick cross-sections were used and given that the permanent deformation observed hardly exceeded 1.5 inches, no substantial traffic-associated changes in properties were expected in the unbound materials across the perpetual test sections on the north side. Since the unbound material layers were adequately protected, no marked trends in terms of GSD or shear strength parameters were anticipated. Furthermore, testing of non-trafficked material from perpetual sections was deemed expendable as it was found reasonable to consider that the post-traffic condition of P-154 subbase material in test section LFP1-N (i.e., the thickest section with 15 inches of P-401) should approach a non-trafficked condition. In addition, only two replicates were initially considered sufficient to get a rough estimate of strength parameters for test sections LFP3-N and LFP4-N, whereas a single test targeting only resilient moduli values for LFC5-N and LFS6-N was considered adequate. Considering that only one sample/replicate was tested in both GSD and triaxial testing, it was unexpected to find the shear strength to correlate well with P-401 surface layer thickness and full-scale traffic test observations.

Table 18 summarizes the triaxial test results for the P-154 subbase material collected from the CC7 north side. The moisture-density condition for each specimen is also included. The moisture content, $w\%$, corresponded to the final value measured upon completion of the test. Table 18 also shows the results of non-linear regression using the universal model. The k_1 , k_2 , and k_3 parameters were intended to be utilized in the future to characterize the non-linear behavior of P-154 material at different states of stress. Along with the regression parameters, predicted resilient moduli, M_R , corresponding to a confining pressure, σ_3 , of 15 psi and a cyclic stress, S_{cyclic} , of 27 psi (12th sequence of resilient modulus test) are included as reference values. Also, the standard error ratio, S_e/S_y , and adjusted coefficient of determination, R^2_{adj} , are included to explain the goodness of fit. Finally, the confining pressure applied during the quick shear test and the corresponding measured maximum vertical stress, σ_{v-max} , is reported.

In table 18, it can be observed that the average resilient moduli values varied between 40,307 psi and 46,869 psi, which was found to be reasonable for P-154 subbase material considering the state of stress used in the prediction and specimen moisture-density condition. Typical values in the literature for subbase materials at optimum conditions in roadways range from 28,000 psi to 37,500 psi (16). Again, the statistical parameters presented in the table indicate that the universal model adequately fits the data. Individual forms reporting the P-154 data generated from the laboratory testing are included in Appendix B. The Mohr-Coulomb failure envelopes were generated for every perpetual test section and are shown in Appendix C.

Table 19 summarizes the estimated strength parameters for trafficked P-154 material in perpetual sections. Details on the quick shear test results and the Mohr-Coulomb envelopes can be found in Appendix C. GSD test results presented before were consistent with findings from post-traffic triaxial testing where decreasing friction angle (ϕ) was observed with decreasing P-401 thickness for sections LFP1-N, LFP2-N, and LFP3-N. In these sections, a similar level of compaction energy from full-scale traffic was imparted. As previously mentioned, breakage of particles in the form of attrition or abrasion leads to increasing particle roundness which in turn decreases the friction angle.

Table 18. Summary of Triaxial Test Results for P-154 Specimens, North Side

Sample	Compaction Condition		Resilient Modulus						Quick Shear	
	w (%)	ρ_{dry} (pcf)	M_R (psi)	k_1	k_2	k_3	S_x/S_y	R^2_{Adj}	σ_3 (psi)	σ_{v-max} (psi)
LFP1-N (T-1)	4.2	133.5	48,146	1,451	0.676	-0.417	0.136	0.98	2.5	133
LFP1-N (T-2)	4.2	134.9	43,934	1,173	0.721	-0.337	0.102	0.99	5	187
LFP1-N (T-3)	4.3	135.5	43,414	1,297	0.683	-0.420	0.116	0.98	10	239
Average			45,165	1,307	0.693	-0.391	0.118	0.98		
LFP2-N (T-1)	4.4	134.0	43,876	1,447	0.671	-0.548	0.157	0.97	2.5	134
LFP2-N (T-2)	4.3	133.7	41,767	1,259	0.550	-0.097	0.195	0.96	5	187
LFP2-N (T-3)	4.2	133.5	39,152	1,054	0.718	-0.344	0.091	0.99	10	226
Average			41,598	1,253	0.647	-0.329	0.148	0.97		
LFP3-N (T-1)	4.2	135.0	48,616	1,416	0.757	-0.570	0.108	0.99	2.5	148
LFP3-N (T-2)	4.2	134.5	43,727	1,151	0.791	-0.491	0.126	0.98	10	220
Average			46,172	1,283	0.774	-0.531	0.117	0.98		
LFP4-N (T-1)	4.3	136.6	52,316	1,320	0.778	-0.393	0.100	0.99	2.5	135
LFP4-N (T-2)	4.2	134.3	44,232	1,297	0.683	-0.420	0.116	0.98	10	230
Average			46,539	1,309	0.731	-0.406	0.108	0.98		
LFC5-N (T-1)	4.2	135.6	46,869	1,168	0.678	-0.117	0.088	0.99	10	239
LFS6-N (T-1)	4.2	135.5	40,307	962	0.663	-0.010	0.221	0.94	10	215

(T-1), (T-2), (T-3): trafficked material-replicate 1, 2, and 3; respectively

Table 19. Summary of Strength Parameters for P-154 Specimens, North Side

Test Section	Strength Parameters	
	Cohesion (psi)	Friction Angle (°)
LFP1-N (T)	20.0	54.5
LFP2-N (T)	21.0	53.2
LFP3-N (T)	24.5	50.0
LFP4-N (T)	21.0	52.4

(T) trafficked material

Not only the cross-section but also the traffic load drives the level of compaction energy imparted to the material and hence, the potential for changes in GSD. Figure 34 illustrates how the change in ϕ correlates with the combined effect of changes in pavement structure and traffic conditions. For instance, under the same traffic condition, the lowest ϕ value among perpetual sections would be expected from LFP4-N since the protection for underlying materials provided by an 8-inch P-401 surface layer is not as effective as a 10-inch or thicker layer. However, although LFP3-N had a thicker P-401 layer compared to LFP4-N, the number of passes underwent by LFP3-N was higher than LFP4-N, increasing the exposure of P-154 material to compaction energy from traffic. Furthermore, over 60% of these additional vehicle passes were applied at a wheel load 18% higher than LFP4-N in magnitude. In the case of LFP1-N and LFP2-N, which were subjected to identical traffic conditions, the observed decrease in ϕ value when going from a 15-inch to a 12-inch P-401

surface layer was limited to roughly one degree. This can be attributed to the relative deficit of surface thickness available to protect the underlying unbound materials. Similar trends can be observed from GSD test results in figures 25(b) and 25(c), where LFP3-N presented the most significant deviation in gradation relative to either the non-trafficked baseline condition or the LFP1-N/LFP2-N trafficked condition. In the same figures, the differences in both percent finer sieves #10 and #40 between LFP1-N and LFP2-N were found to be negligible.

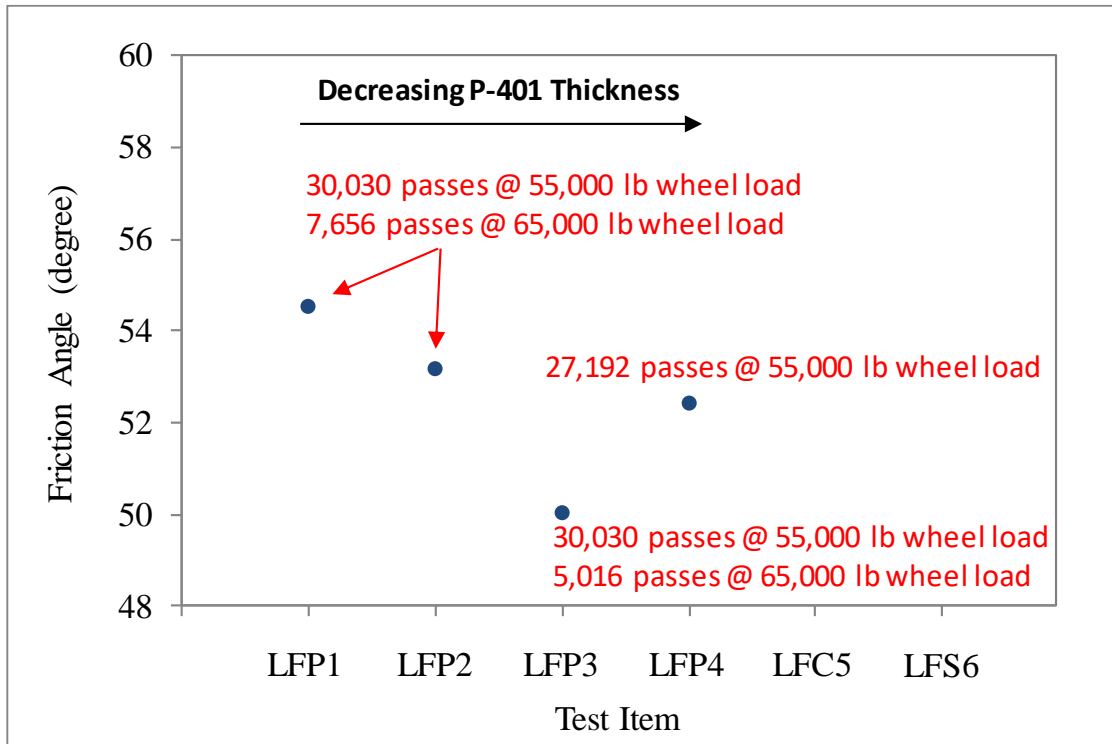


Figure 34. Changes in Friction Angle for P-154 Material in Perpetual Sections, North Side

5.2.2.3 P-154 Subbase Material in Overload Test Sections (South Side)

Overall, the post-traffic triaxial testing of P-154 material from overload test sections generated the most comprehensive dataset in this laboratory program. Three resilient modulus replicates, each followed by a quick shear test, were conducted using trafficked material from every overload test section and non-trafficked material from limited test sections. Table 20 summarizes the triaxial test results for the CC7 south side. Similar to the North side, predicted resilient moduli values correspond to a confining pressure, σ_3 , of 15 psi and a cyclic stress, S_{cyclic} , of 27 psi (12th sequence of resilient modulus test). In table 20, it can be observed that the average predicted resilient moduli values ranged from 39,587 psi to 44,311 psi. This range was believed to be reasonable. Regression constant sets for the predictive universal model (i.e., k_1 , k_2 , and k_3 parameters) are provided for each individual replicate. As shown by the statistical parameters in the table (i.e., S_e/S_y , and R^2_{adj}), the universal model fits the data quite well. Individual test reports that include resilient modulus and quick shear data for every single test are included in Appendix B.

Table 20. Summary of Triaxial Test Results for P-154 Specimens, South Side

Specimen	Compaction Condition		Resilient Modulus					Quick Shear		
	ρ_{dry} (pcf)	w (%)	M_R (psi)	k_1	k_2	k_3	S_e/S_y	R^2_{Adj}	σ_3 (psi)	σ_{v-max} (psi)
LFC1-S (NT-1)	133.0	4.0	44,540	1,233	0.662	-0.246	0.134	0.98	2.5	141
LFC1-S (NT-2)	133.4	4.0	43,143	1,055	0.827	-0.465	0.127	0.98	5	158
LFC1-S (NT-3)	132.5	4.1	41,481	1,088	0.763	-0.415	0.124	0.98	10	229
Average			43,054	1,125	0.751	-0.375	0.128	0.98		
LFC1-S (T-1)	133.7	4.1	43,033	1,433	0.679	-0.583	0.178	0.96	5	156
LFC1-S (T-2)	133.5	4.2	48,748	1,342	0.792	-0.567	0.155	0.97	10	191
LFC1-S (T-3)	132.5	4.2	41,153	1,139	0.719	-0.389	0.116	0.98	15	231
Average			44,311	1,305	0.730	-0.513	0.150	0.97		
LFC2-S (T-1)	132.1	4.2	41,195	973	0.784	-0.303	0.101	0.99	5	138
LFC2-S (T-2)	131.9	4.0	42,201	1,149	0.711	-0.344	0.122	0.98	10	181
LFC2-S (T-3)	132.8	4.0	44,275	897	0.907	-0.368	0.076	0.99	15	236
Average			42,557	1,007	0.801	-0.338	0.100	0.99		
LFC3-S (T-1)	136.2	4.3	44,031	1,189	0.679	-0.249	0.073	0.99	5	134
LFC3-S (T-2)	134.2	4.6	39,217	1,011	0.700	-0.226	0.086	0.99	10	167
LFC3-S (T-3)	133.7	4.3	43,148	1,325	0.647	-0.373	0.152	0.98	15	204
Average			42,132	1,175	0.676	-0.283	0.104	0.99		
LFC4-S (T-1)	133.1	4.2	41,403	1,332	0.664	-0.490	0.182	0.96	5	144
LFC4-S (T-2)	132.4	4.2	44,227	1,405	0.662	-0.464	0.134	0.98	10	192
LFC4-S (T-3)	135.9	4.3	45,152	1,400	0.651	-0.397	0.168	0.97	15	246
Average			43,594	1,379	0.659	-0.450	0.161	0.97		
LFC5-S (T-1)	133.1	4.0	40,886	1,091	0.711	-0.310	0.100	0.99	5	130
LFC5-S (T-2)	135.0	4.1	36,323	805	0.710	-0.010	0.203	0.95	10	178
LFC5-S (T-3)	134.2	4.1	38,287	971	0.747	-0.321	0.118	0.98	15	215
Average			39,587	1,031	0.729	-0.316	0.109	0.99		
LFC6-S (T-1)	135.3	4.2	40,377	1,028	0.732	-0.288	0.091	0.99	5	137
LFC6-S (T-2)	134.1	4.5	41,328	1,425	0.628	-0.510	0.206	0.95	10	165
LFC6-S (T-3)	134.9	4.5	41,940	1,216	0.722	-0.472	0.180	0.96	15	208
Average			41,634	1,321	0.675	-0.491	0.193	0.96		

(T-1), (T-2), (T-3): trafficked material-replicate 1, 2, and 3; respectively

(NT-1), (NT-2), (NT-3): non-trafficked material-replicate 1, 2, and 3; respectively

Although the gear load on the south side never exceeded the load imparted to the perpetual test sections, the unbound materials in the overload test sections were protected only by 3 inches of P-401 surface course. Furthermore, surface rut depths ranging between 3 inches and 6 inches were observed in the overload test sections whereas the values measured in the perpetual test sections were all below 2 inches. Consequently, possible overload effects on changes in P-154 material strength resulting from particle breakage, if any, were expected to be more significant than that on perpetual test sections.

The quick shear test data reported in table 20 revealed the presence of two marked trends in the change of maximum vertical stress, σ_{v-max} , with traffic conditions. An example of these trends is presented in figure 35(a) and figure 17(b). In both figures, data from quick shear tests conducted at a confining pressure of 10 psi is presented for every single test section. The non-trafficked

baseline condition corresponded to test section LFC1-S. In both cases, the non-trafficked condition presented the highest σ_{v-max} . For LFC1-S to LFC3-S test sections, σ_{v-max} decreased with decreasing wheel load whereas for LFC4-S to LFC6-S test sections, σ_{v-max} decreased with increasing wheel load. A similar trend was generally observed at other levels of confinement.

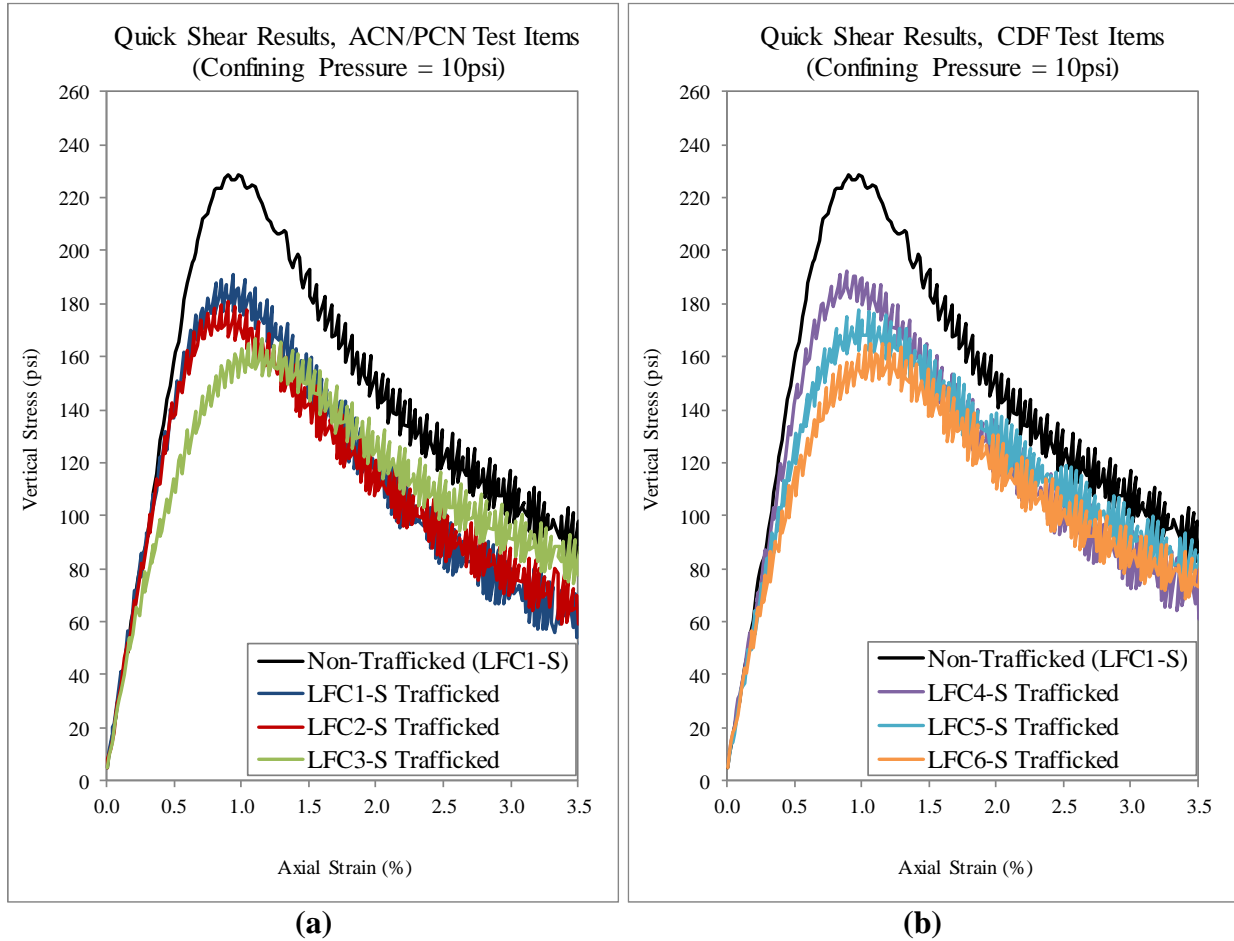


Figure 35. Effect of Overload Traffic on the Post-Traffic Maximum Vertical Stress: (a) LFC1-S to LFC3-S Test Sections, (b) LFC4-S to LFC6-S Test Sections

To further investigate the observed trends, the shear strength parameters were estimated and are summarized in table 21. In table 21, the same trend observed for σ_{v-max} in figure 35 is replicated in terms of ϕ . Details of the Mohr-Coulomb failure envelopes can be found in Appendix C.

Regardless of some observable differences in the cohesion value between the overload test sections, the direct comparison of the Mohr-Coulomb failure envelopes presented in figure 36 was consistent with the trends observed in figure 35, in terms of σ_{v-max} , and table 21, in terms of ϕ . In both figure 36(a) and figure 36(b), the strength deficit in trafficked P-154 material was captured by a downward shifting of the failure envelopes with respect to the non-trafficked baseline condition. Such trends were consistent with the observed performance (i.e.; rut depth) of overload test sections and the GSD test results reported in previous sections.

Table 21. Summary of Strength Parameters for P-154 Specimens, South Side

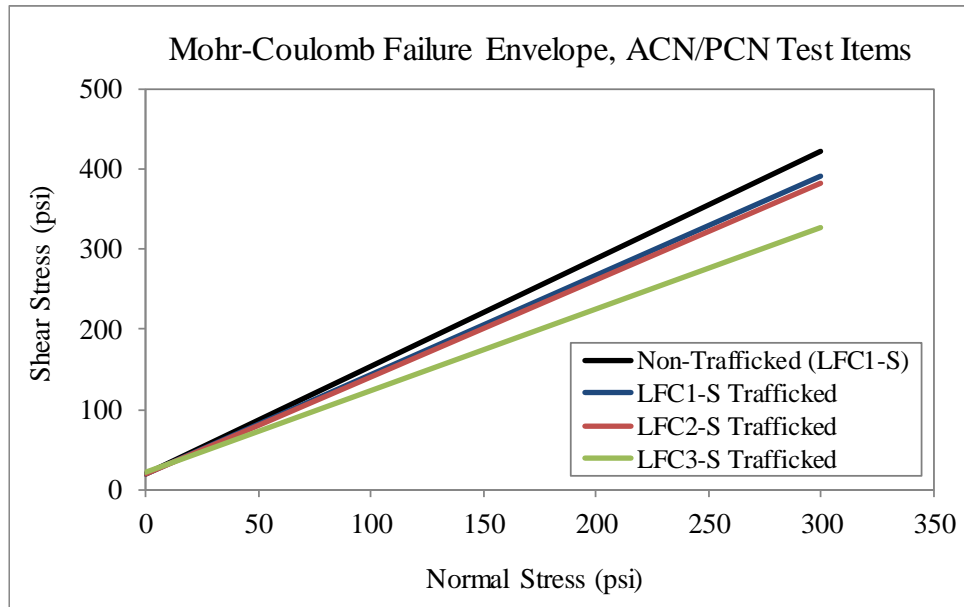
Test Section	Strength Parameters	
	Cohesion (psi)	Friction Angle (°)
LFC1-S (NT)	20.0	53.3
LFC1-S (T)	20.0	51.1
LFC2-S (T)	19.0	50.4
LFC3-S (T)	22.0	45.5
LFC4-S (T)	19.5	51.3
LFC5-S (T)	19.0	48.9
LFC6-S (T)	20.0	47.0

(T) trafficked material

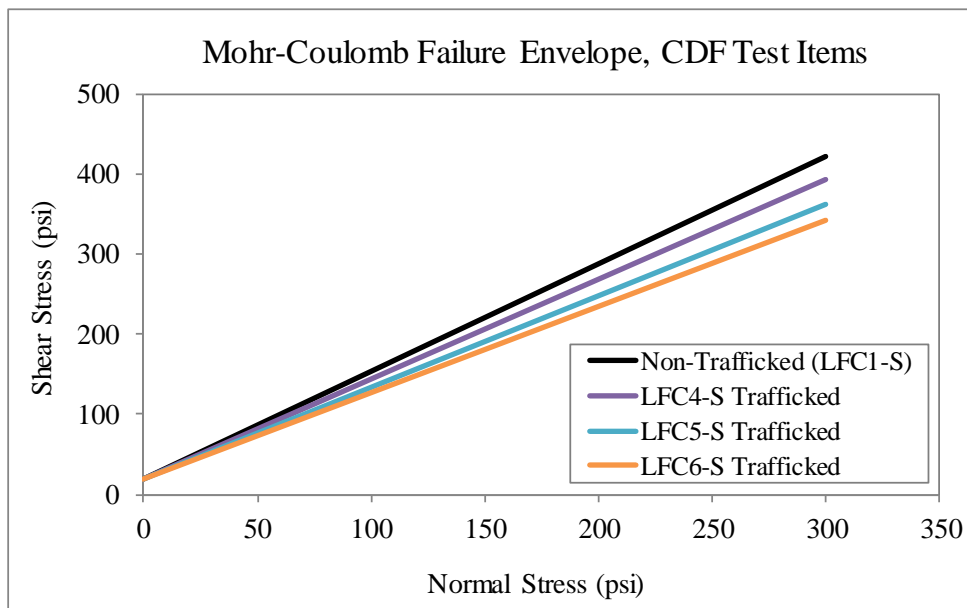
(NT) non-trafficked material

The ϕ values reported in table 21 are illustrated in figure 37. The trends of strength deficit in P-154 material relative to the baseline condition (i.e., LFC1-S non-trafficked) corresponded to increasing gear load for test sections LFC1-S to LFC3-S and increasing wheel load for test sections LFC4-S to LFC6-S. However, besides the difference in load magnitude between test sections LFC1-S to LFC3-S and LFC4-S to LFC6-S, the difference in the number of wanders applied during overload sequences also determined the level of compaction energy imparted to P-154 material in each test section. The trends observed for ϕ were consistent with those of post-traffic gradation reported for P-154 material. As noted in figure 30, the post-traffic fines content increased from test sections LFC1-S to LFC3-S and from LFC4-S to LFC6-S. Is it known that particle breakage in the form of abrasion promotes increasing roundness of particles and hence, decreasing friction angle. From this perspective, the results from both GSD and triaxial testing were found to be consistent and mirrored the overload effects.

As previously discussed, the field overload observations in terms of pavement performance agreed with the laboratory test results. As shown in figure 31, the trend in accumulated surface rut depth at pass #14,520 observed for all overload test sections mirror the trend of changes in ϕ shown in figure 37. The test sections presenting more accumulation of permanent deformation were subjected to higher levels of compaction energy imparted by traffic. The severity of particle breakage increased with the level of compaction energy imparted by traffic, resulting in increased potential for loss of strength in terms of friction angle. These trends in accumulated permanent deformation observed from surface rut depth measurements were confirmed during CC7 post-traffic trenching. Figure 38 shows estimates of permanent deformation by material for all overload test sections. These preliminary calculations were obtained from post-traffic layer profiles measured during trenching. Note that the surface rut depth measurements presented in figure 31 show a snapshot of the pavement damage at a given time prior to the test completion whereas the permanent deformation estimates shown in figure 38 capture the total damage induced to the P-154 material by the overloads. When correlating both figures, it can be said that these trends were consistent with trends observed for ϕ in figure 37.



(a)



(b)

Figure 36. Comparison of Mohr-Coulomb Failure Envelopes for Post-Traffic P-154 Subbase: (a) LFC1-S to LFC3-S, (b) LFC4-S to LFC6-S

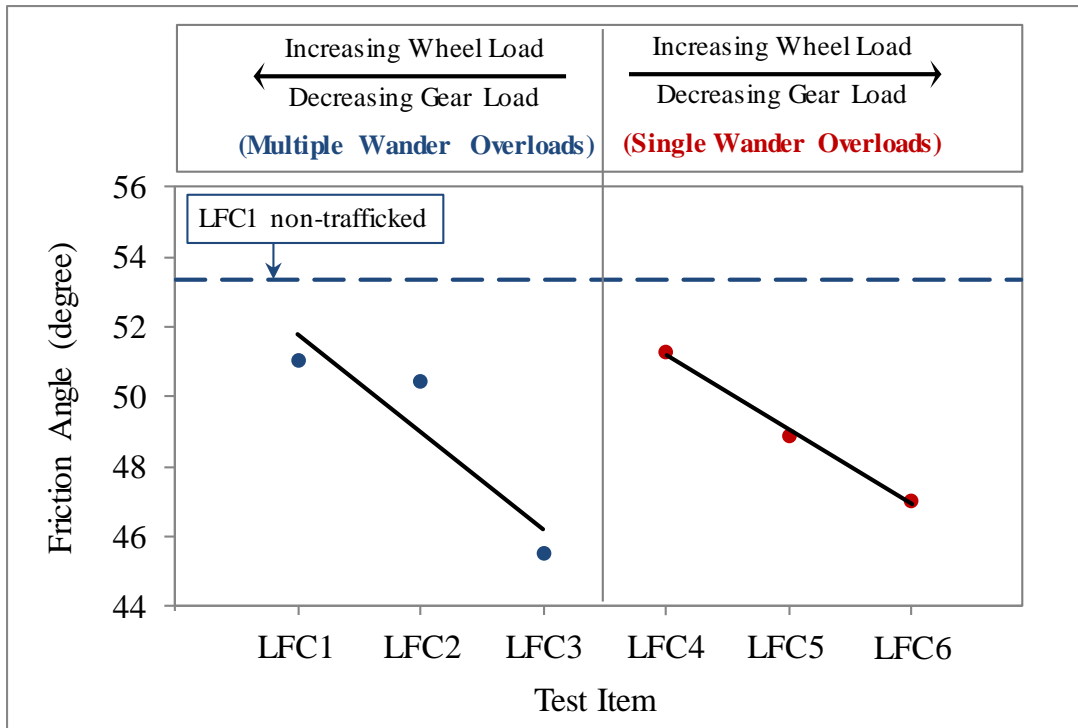


Figure 37. Changes in Friction Angle for P-154 Subbase in Overload Sections, South Side

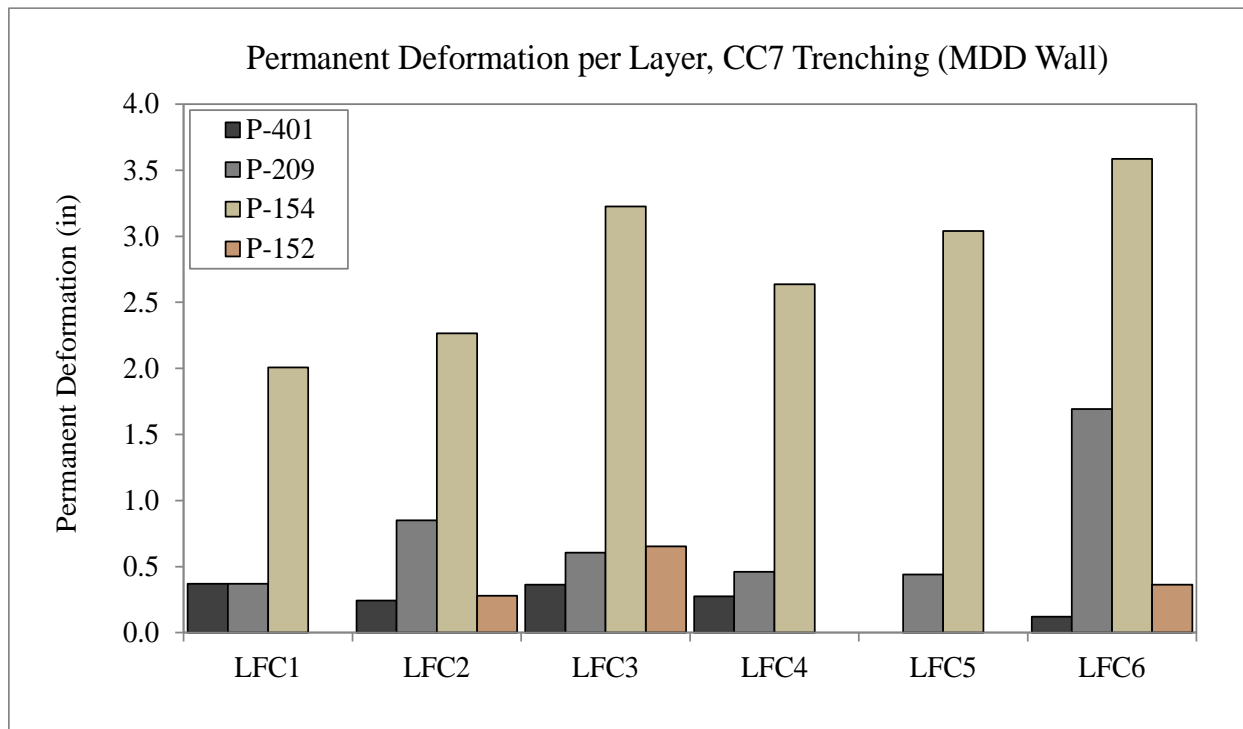


Figure 38. Estimated Permanent Deformation from CC7 Post-Traffic Layer Profile Measurement

5.2.2.4 P-154 Subbase Material in Overload Test Sections (South Side) - 6×12 in. Specimens

A friction angle value of 44° for P-154 material has been reported in the literature (17, 18). Although the moisture-density conditions for the specimens tested in these studies were not detailed, maximum dry density and optimum moisture content values of 129 pcf and 6.5%, respectively, were reported. A friction angle of 49° at similar moisture-density conditions were also reported during Construction Cycle 1 at the NAPTF database (14). Thus, it is reasonable to expect values equal or greater than 49° for denser P-154 specimens at lower moisture content as was the case of CC7. Considering the moisture-density condition used in the present study, a reasonable ϕ range for this type of material should fall between the higher 40s and lower 50s. The friction angles measured for the P-154 material were examined. From tables 19 and 21, the measured ϕ values for the P-154 material were found to range between 46° and 55° with a total average of 50.7°.

Besides the moisture-density condition, the sample size and/or compaction method could play an important role. To verify sample size and compaction method effects, the laboratory testing program included additional testing of a limited number of large P-154 specimens (i.e., 6-inch diameter by 12-inch height) using a large MTS triaxial system rather than the medium IPC triaxial frame. This time, P-154 specimens were compacted using the vibratory hammer. A total of four additional large specimens of P-154 trafficked material from LFC4-S and LFC6-S items were tested. Testing of two additional specimens per test section was expected to provide adequate information to obtain a rough estimate of friction angle in large P-154 samples. As shown in table 22, considering LFC6-S (T-2) as an outlier in terms of resilient modulus, the moduli values ranged from 35,309 psi to 38,340 psi. This range was lower than that observed in small P-154 specimens (i.e., table 20), and therefore suggested a possible effect of sample size and compaction method on the resilient response of the material. Also, the difference in the resilient deformation measuring mechanism between both triaxial systems can be considered a potential source of discrepancy.

Table 22. Summary of Triaxial Test Results for Large P-154 Specimens (6×12 in.), South Side

Specimen	Compaction Condition		Resilient Modulus					Quick Shear		
	ρ_{dry} (pcf)	w (%)	M_R (psi)	k_1	k_2	k_3	S_e/S_y	R^2_{Adj}	σ_3 (psi)	σ_{v-max} (psi)
LFC4-S (T-1)	4.2	133.6	38,340	792	0.817	-0.171	0.086	0.99	5	52
LFC4-S (T-2)	3.9	133.3	37,494	683	0.871	-0.107	0.071	0.99	10	96
Average			37,917	738	0.844	-0.139	0.078	0.99		
LFC6-S (T-1)	4.3	133.3	35,309	616	0.954	-0.248	0.076	0.99	5	76
LFC6-S (T-2)	4.0	133.4	22,105	741	0.449	-0.010	0.330	0.87	15	131
Average			28,707	678	0.702	-0.129	0.203	0.93		

(T-1), (T-2): trafficked material-replicate 1, 2, and 3; respectively

The quick shear test data was used to estimate the strength parameters as shown in table 23. Figure 39 illustrates the difference in ϕ value between LFC4-S and LFC6-S for P-154 large specimens. Although the ϕ values were consistently lower than those observed in small specimens, the trends remained consistent regardless of sample size and compaction method. In other words, the ϕ value decreased from LFC4-S to LFC6-S with increasing wheel load. However, the quick shear test results in LFC4-S and LFC6-S small specimens overestimated the ϕ value by 1° and 2.5°,

respectively, relative to the values obtained from large specimens compacted with a vibratory hammer. The average ϕ value obtained from large specimens was 47.4° . The range of values presented in table 23, was found to be in closer agreement with the literature (14, 17, and 18) than the range obtained from small specimens.

Table 23. Summary of Strength Parameters for Large P-154 Specimens (6×12 in.), South Side

Test Section	Strength Parameters	
	Cohesion (psi)	Friction Angle ($^\circ$)
LFC4-S (T)	2.8	50.3
LFC6-S (T)	9.5	44.5

(T) trafficked material

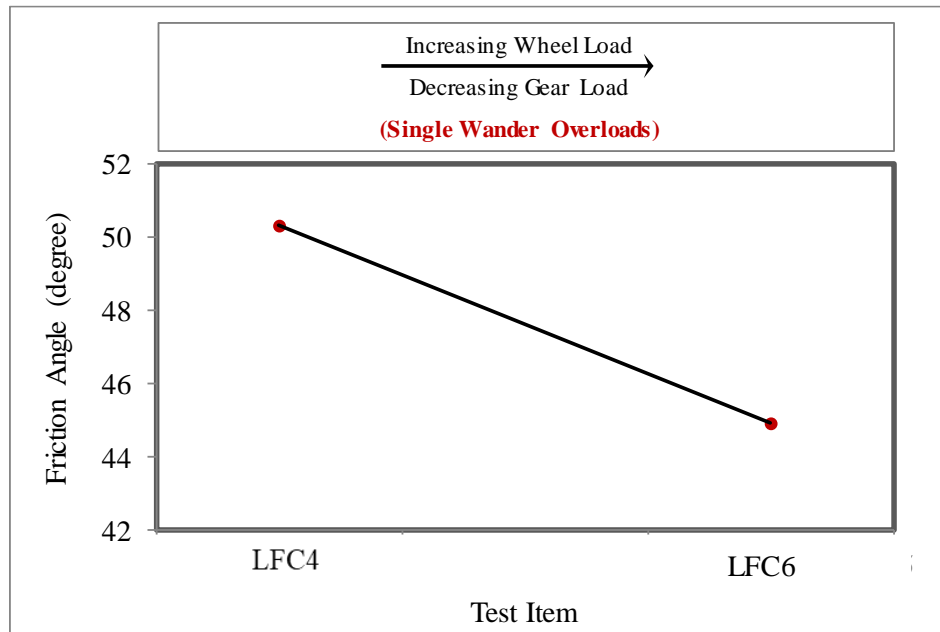


Figure 39. Changes in Friction Angle for P-154 Large Specimens (6×12 in.), South Side

The possibility of malfunctioning components in both the MTS and the IPC triaxial systems was ruled out after verifying the accuracy of load cells and confining pressure transducers. The discrepancy in response between the two systems was deemed to be negligible. The potential effect of sample size and compaction method observed on the measured strength of unbound materials should be considered in future laboratory data analysis efforts.

5.3 OBSERVATIONS

The following key observations were made based on the outcome of the CC7 post-traffic laboratory testing program:

a. General

- There was consistency between GSD and triaxial test results in both P-154 and P-209 material.
- Besides showing high correspondence to each other, the GSD and triaxial test results on P-154 materials also confirmed the field performance captured by surface rut depth measurements, and examination during CC7 post-traffic trenching. However, the same was not observed for P-209 material.
- Some discrepancy between friction angle values obtained from P-154 small and large specimens was observed. Possible sources of such discrepancy were the specimen size and compaction method.

b. GSD and triaxial test results of P-154 aggregate base

- North Side: The observed differences in gradation corresponded to the degree of exposure to damage imposed by the varying pavement structure, and to the specific traffic history in each particular perpetual test section. Such differences indicate possible particle breakage in the form of attrition or abrasion.
- South Side: The observed differences in gradation corresponded to the changes in traffic conditions across test sections imposed by the overloads. Such differences indicate possible particle breakage in the form of abrasion.
- In both the north and south sides, these particle breakage mechanisms promote increasing particle roundness which leads to the loss of particle interlock. This was found to be consistent with the triaxial test results that showed a decrease in friction angle with increasing level of exposure to compaction energy imparted by traffic.

c. GSD and triaxial test results of P-209 aggregate base

- No differences in gradation, modulus, and shear strength parameters that corresponded to the changes in overload traffic conditions across test sections were observed.

6. P-152 SUBGRADE SOIL

6.1 SAMPLE COLLECTION

One undisturbed P-152 subgrade sample per test section was collected from trafficked areas using 12-inch Shelby tubes. Shelby tube sampling was conducted in select non-trafficked test sections in accordance with the *CC7 Post-Traffic Trenching and Test Plan* (see Appendix A). A total of 14 Shelby tube samples were available only for triaxial testing.

6.1.1 Triaxial Specimen Preparation

The P-152 undisturbed specimens collected in Shelby tubes were extruded and trimmed to the required triaxial testing height of 5.6 inches. Therefore, the specimens were tested for resilient modulus and quick shear at actual field conditions.

6.2 TEST RESULTS

Triaxial testing was conducted on P-152 undisturbed specimens in accordance with AASHTO T307 standard. The resilient modulus test was performed on all specimens followed by the quick shear test. Different from base and subbase materials, a single replicate per test section of trafficked P-152 subgrade soil was conducted. In addition, a single non-trafficked P-152 subgrade soil specimen was tested for the north and south side. The quick shear test was conducted at zero confining pressure to obtain the unconfined compressive strength (UCS) of the material. A total of 14 triaxial tests were performed. As discussed in section 5.2.2, the resilient modulus test data was fitted to the generalized enhanced version of the widely known universal model (16).

Table 24 summarizes the triaxial test results for P-152 subgrade soil. The average resilient modulus for the south overload test sections was 5,624 psi, whereas for the north side perpetual and drainable base test sections it was 7,633 psi. In other words, the subgrade on the north side was found to be stiffer than the south side, on average. It is worth mentioning that the state of stress considered for estimating the reported moduli values corresponds to 6 psi of confining stress, σ_3 , and 9 psi of cyclic stress, S_{cyclic} . The average UCS for the north side was found to be 21 psi, whereas for the south side it was 20 psi. In terms of UCS, the difference in average values between the north and south sides was minimal.

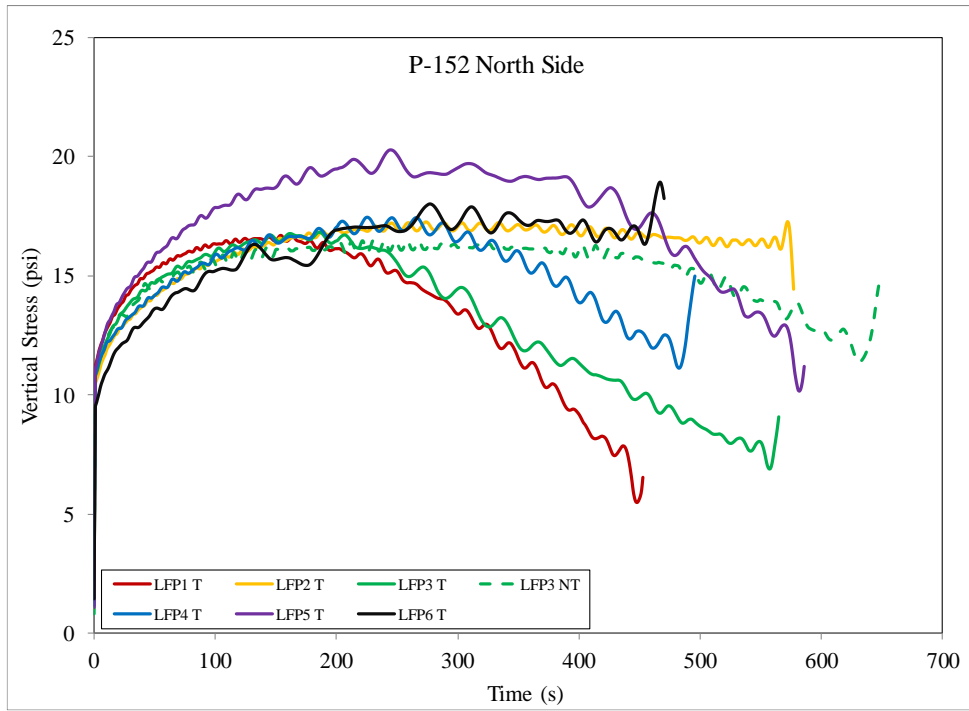
Figure 40(a) and figure 40(b) illustrate the quick shear test results for the north and south side respectively. Although the average UCS for the north and south side were similar, figure 40(a) revealed that the subgrade strength on the north side is relatively uniform throughout all test sections. On the south side, the variation in UCS was significantly higher as observed in figure 40(b). In general, no obvious effect of the varying pavement structure and specific traffic history in the north side, and changes in traffic conditions imposed by the overloads in the south side; was observed.

Table 24. Summary of Triaxial Test Results for P-152 Specimens, North and South Side

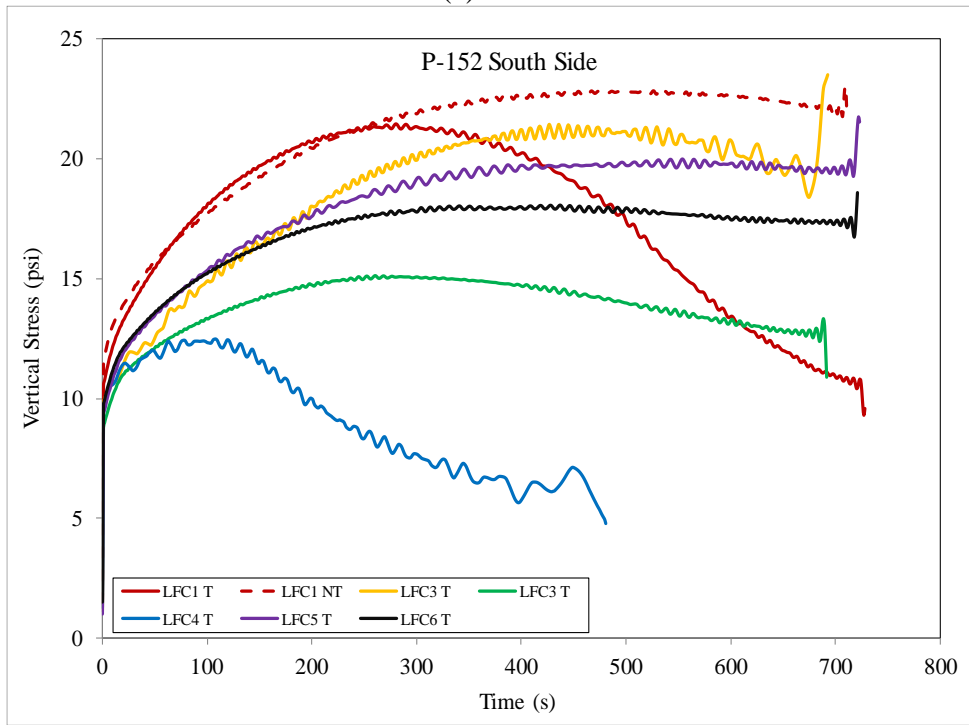
Sample	Moisture-Density Condition		Resilient Modulus						UCS
	ρ_{dry} (pcf)	w (%)	M_R (psi)	k_1	k_2	k_3	S_e/S_y	R^2_{Adj}	σ_{v-max} (psi)
LFC1-S (T)	97.2	27.1	5,433	884	0.227	3.969	0.170	0.97	23
LFC2-S (T)	95.0	27.0	7,154	1,229	0.271	4.287	0.201	0.95	26
LFC3-S (T)	97.4	26.6	3,604	954	0.276	6.001	0.259	0.92	16
LFC4-S (T)	96.1	28.0	6,442	1,389	0.400	5.492	0.184	0.96	15
LFC5-S (T)	95.8	27.4	4,402	1,053	0.348	5.775	0.132	0.98	22
LFC6-S (T)	96.6	27.5	4,525	917	0.241	4.865	0.179	0.96	20
LFC6-S (NT)	98.7	25.3	7,807	745	0.228	1.873	0.221	0.97	25
Average	96.7	27.0	5,624	1,025	0.284	4.609	0.192	0.96	21
LFP1-N (T)	87.5	32.3	7,633	1,228	0.138	3.715	0.159	0.97	18
LFP2-N (T)	87.6	32.3	6,110	1,108	0.200	4.332	0.186	0.96	19
LFP3-N (T)	86.8	34.1	6,704	1,160	0.195	4.136	0.184	0.96	19
LFP3-N (NT)	88.0	32.4	8,889	1,308	0.308	3.769	0.114	0.99	20
LFP4-N (T)	82.6	36.3	8,531	945	0.217	2.436	0.262	0.94	20
LFP5-N (T)	95.5	27.6	6,840	1,048	0.255	3.802	0.125	0.99	22
LFP6-N (T)	95.0	27.2	5,116	902	0.327	4.523	0.144	0.98	20
Average	89.0	31.7	7,118	1,100	0.234	3.816	0.168	0.97	20

(T) trafficked material

(NT) non-trafficked material



(a)



(b)

Figure 40. Unconfined Compressive Strength of P-152 Subgrade: (a) North Side, (b) South Side

6.3 OBSERVATIONS

- The resilient modulus of the subgrade on the north side was higher than the south side, which confirms a stiffer subgrade on the north side test sections. This observation was consistent with the target CC7 CBR values: 5.5 and 5.0 for the north and south side, respectively.
- The difference between north and south side in terms of unconfined compressive strength was minimal. The subgrade strength of the north side was more uniformly distributed, whereas on the south side a relatively high coefficient of variation was observed.
- Based on the triaxial test results, there was no observable effect of the varying pavement structure and specific traffic history in the north side, and changes in traffic conditions imposed by the overloads in the south side.

7. REFERENCES

1. Aponte, R., and Budesá, C., National Airport Pavement Test Facility (NAPTF) Construction Cycle Seven (CC-7) History Report, 2016.
2. Yin, H., Cary, C.E., Wang, Z., Li, Q., Augustyn, S., and Davis, J. Construction Cycle 7 Test Report – Perpetual Test, 2017.
3. Yin, H., Cary, C.E., Wang, Z., Li, Q., Augustyn, S., and Davis, J. Construction Cycle 7 Test Report – Overload Test, 2017.
4. Harvey, J.T., Hoover, T.P., Coetzee, N.F., and Monismith, C.L. Rutting Evaluation of Asphalt Pavements Using Full-scale Accelerated Load and Laboratory Performance Tests, 2002.
5. Skok, E., Johnson, E., and Turk, A. Asphalt Pavement Analyzer (APA) Evaluation, *MN/RC Report 2003-02*, 2002.
6. Rushing, J., Little, D., and Garg, N. Asphalt Pavement Analyzer Used to Assess Rutting Susceptibility of Hot-Mix Asphalt Designed for High Tire Pressure Aircraft, *Journal of the Transportation Research Board*, Vol. 2296, pp. 97-105, 2012.
7. NCAT. Performance Testing of HMA Presentation, 2016.
8. Federal Aviation Administration. AC 150/5370-10C, *Airport Construction Standards*, 2014.
9. Bonaquist, R. F. Refining the Simple Performance Tester for Use in Routine Practice, *NCHRP Report 614*, Transportation Research Board, National Research Council, Washington, D.C., 2008.
10. Garg, N., Bennert, T., and Brar, H. Performance of Hot Mix Asphalt Surface Under High Tire Pressure Aircraft Landing Gear Configuration at the FAA National Airport Pavement Test Facility.
11. National Cooperative Highway Research Project, *NCHRP Project 1-28A: Harmonized Test Methods for Laboratory Determination of Resilient Modulus for Flexible Pavement Design*, Research Results Digest, No 285, Transportation Research Board of the National Academies, Washington, D.C., 2004.

12. Vallejo, L.E. Interpretation of the Limits in Shear Strength in Binary Granular Mixtures. *Canadian Geotechnical Journal*, Vol. 38, pp. 1097-1104, 2001.
13. Xiao, Y., Tutumluer, E., Qian, Y., and Siekmeier, J. A. Gradation Effects Influencing Mechanical Properties of Aggregate Base-Granular Subbase Materials in Minnesota, *Journal of the Transportation Research Board*, Vol. 2267, pp. 14-26, 2012.
14. NAPTF Construction Cycle 1 Database, link: <http://www.airporttech.tc.faa.gov/Airport-Pavement/National-Airport-Pavement-Test-Facility-/NAPTF-Databases/CC-1>
15. Daouadji, A, and Hicher, P. Y. An enhanced constitutive model for crushable granular materials, *International Journal for Numerical and Analytical Methods in Geomechanics*, No. 6, Vol. 34, pp. 555-580, 2010.
16. National Cooperative Highway Research Project, *NCHRP Project 1-37A: Guide for Mechanistic-Empirical Design of New and Rehabilitated Pavement Structures*, Final Report, Part 2, Design Inputs, Transportation Research Board of the National Academies, Washington, D.C., 2004.
17. Xiao, Y., and Tutumluer, E. Best Value Granular Material for Road Foundations, Final Report: MN/RC 2012-01, Minnesota Department of Transportation, Minnesota, 2012.
18. Kim, I. T., and Tutumluer, E. Predicting Rutting Performance of Pavement Granular Layers at the FAA's National Airport Pavement Test Facility. FAA Worldwide Airport Technology Transfer Conference, Atlantic City, New Jersey, 2004.